CLIMB: Data Foundations for Large Scale Multimodal Clinical Foundation Models

Wei Dai [1] **Peilin Chen** [1] **Malinda Lu** [1] **Daniel Li** [1] **Haowen Wei** [2] **Hejie Cui** [3] **Paul Pu Liang** [1]

Abstract

Recent advances in clinical AI have enabled remarkable progress across many clinical domains. However, existing benchmarks and models are primarily limited to a small set of modalities and tasks, which hinders the development of large-scale multimodal methods that can make holistic assessments of patient health and well-being. To bridge this gap, we introduce Clinical Large-scale Integrative Multimodal Benchmark (CLIMB), a comprehensive clinical benchmark unifying diverse clinical data across imaging, language, temporal, and graph modalities. CLIMB comprises 4.51 million patient samples totaling 19.01 terabytes distributed across 2D imaging, 3D video, time series, graphs, and multimodal data. Through extensive empirical evaluation, we demonstrate that multitask pretraining significantly improves performance on understudied domains, achieving up to 29% improvement in ultrasound and 23% in ECG analysis over single-task learning. Pretraining on CLIMB also effectively improves models' generalization capability to new tasks, and strong unimodal encoder performance translates well to multimodal performance when paired with task-appropriate fusion strategies. Our findings provide a foundation for new architecture designs and pretraining strategies to advance clinical AI research. Code is released at this link.

1. Introduction

Advances in AI for clinical data have significantly helped doctors process and analyze complex clinical information for diagnosis, treatment planning, and decision support (Esteva et al., 2019; Huang et al., 2019; Rajpurkar et al., 2022). These domains include analyzing clinical images (Johnson et al., 2019; Irvin et al., 2019a), processing clinical notes

(Huang et al., 2019; Johnson et al., 2016), and predicting patient outcomes (Yan et al., 2024). Despite these achievements, most current approaches remain limited to a few modalities primarily in the image and text domain (Thakoor et al., 2019; Jing et al., 2023b; Sharma et al., 2022), failing to capture the interactions between many medical indicators that clinicians routinely combine to make holistic assessments on patient health and well-being (Liang et al., 2024b; Rajendran et al., 2023; Shaik et al., 2024).

To develop the next generation of holistic multimodal clinical foundation models, we introduce Clinical Large-scale Integrative Multi-modal Benchmark (CLIMB), a comprehensive multimodal clinical benchmark that unifies data across imaging, language, temporal, and genomic modalities. Our dataset comprises 4.51 million patient samples, totaling 19.01 terabytes of data, with a diverse spectrum of modalities: 707K 2D imaging data (including X-rays, dermoscopy images, fundus images, and pathology slides), 1.83M 3D or video samples (ultrasounds, CT scans, endoscopic images and MRI images), 871K 1D data (electronic health records, EEG, ECG, gait and genomic data), 69.3K graph data (brain networks, molecules) and 1.03M multimodal data combining multiple of the above modalities. We accomplish this through a novel data collection and preprocessing pipeline that standardizes diverse data formats from 33 different medical institutions while preserving the natural patterns of missing data. The dataset encompasses 96 different clinical conditions across 13 clinical domains, making it one of the largest and most diverse public clinical benchmarks to date.

Through extensive empirical evaluation on CLIMB, we establish comprehensive benchmarks and best practices for clinical multimodal learning. As illustrated in Fig. 3, our analysis yields three key insights:

1. **Multitask pretraining:** We evaluate single encoders trained jointly on all tasks within each modality in CLIMB. Our experiments show that multitask pretraining significantly improves performance across clinical tasks, achieving up to 32.54% AUC improvement in COVID ultrasound and other understudied areas. Furthermore, pretraining on CLIMB drastically improves model performance in novel and understudied tasks for

---

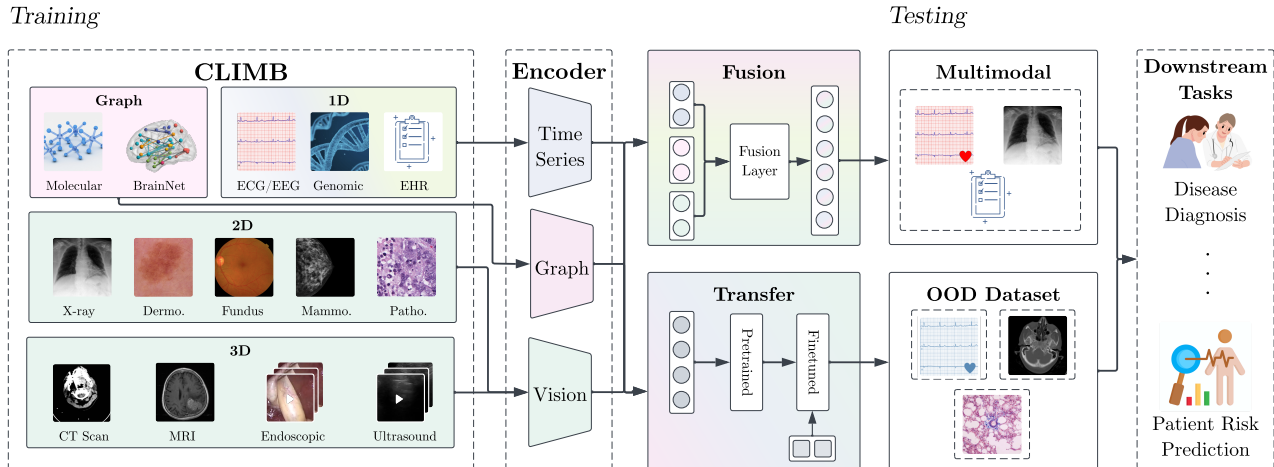arXiv:2503.07667v2 [cs.LG] 20 Mar 2025

Figure 1. **Overview of the CLIMB framework for training and testing multimodal datasets.** The training phase incorporates diverse data modalities: graphs (molecular, BrainNet), 1D signals (ECG/EEG, genomics, EHR), 2D images (X-rays, dermoscopy, fundus, mammograms, pathology), and 3D scans (CT, MRI, endoscopy, ultrasound). Through multitask training on heterogeneous clinical data, our framework enhances model performance across individual tasks, particularly for understudied modalities defined in Fig. 2(b). This approach improves both generalization to novel tasks and multimodal understanding when combined with appropriate fusion strategies, ultimately advancing performance on critical clinical applications like disease diagnosis and patient risk prediction.

general-domain encoders, specialized clinical encoders, and clinical large vision language models (LVLMs).

2. **Few-shot transfer:** We test how models pretrained on CLIMB generalize to new clinical tasks with limited labeled data. Models pretrained on CLIMB demonstrate significant improvements in few-shot learning scenarios, achieving up to 29% improvement in ultrasound and 23% in ECG tasks under few-shot settings compared to pretraining on existing datasets.

3. **Multimodal fusion:** Finally, we investigate different strategies for combining multimodal clinical data, including imaging, text, and time series on MIMIC-IV, a multimodal clinical benchmark. Our results show that single-modality pretraining on CLIMB enhances multimodal learning performance, leading to successful transfer to MIMIC-IV, and that complex fusion strategies perform better on challenging tasks.

In light of these findings, we release our vision, EEG, and ECG unimodal and multimodal models trained on CLIMB, which achieve state-of-the-art performance on multiple clinical tasks. We also provide detailed recommendations for model architecture selection and pretraining strategies across clinical modalities, establishing a practical framework for future clinical AI development. All code for data collection, training, evaluation, and pretrained weights is available at this link.

2. Related Work

We cover related work in unimodal and multimodal clinical benchmarks and models.

2.1. Unified Multimodal Clinical Benchmarks

The convergence of computational advances and large clinical datasets (Johnson et al., 2016; 2019; Irvin et al., 2019a) has enabled AI systems to match human performance across various medical tasks, from retinopathy detection to drug discovery (Tsiknakis et al., 2021; Sone et al., 2021; Rajkomar et al., 2019). While large-scale multimodal foundation models have shown promise in learning unified clinical representations (Liang et al., 2024a; Yang et al., 2024; Philiastides et al., 2021), current benchmarks typically focus on limited modalities like X-rays, pathology, or their combinations (Moses, 2021; Schneider et al., 2022; Nasir et al., 2023). Large benchmarks include BenchMD (Wantlin et al., 2023) and CARES (Xia et al., 2024), covering 7 clinical modalities (1D, 2D, and 3D) and 16 different 2D and 3D image modalities, respectively. As shown in Table 1, however, our dataset uniquely incorporates time series and graph data alongside traditional clinical imaging while maintaining the widest coverage across each of the modalities.

2.2. Multimodal Clinical Models

Recent clinical AI models broadly fall into two categories: LLM-based multimodal systems and specialized vision encoders. LLM-based approaches like Llava-Med (Li et al., 2023) and Med-Flamingo (Moor et al., 2023) combine frozen vision encoders with language models for clinical
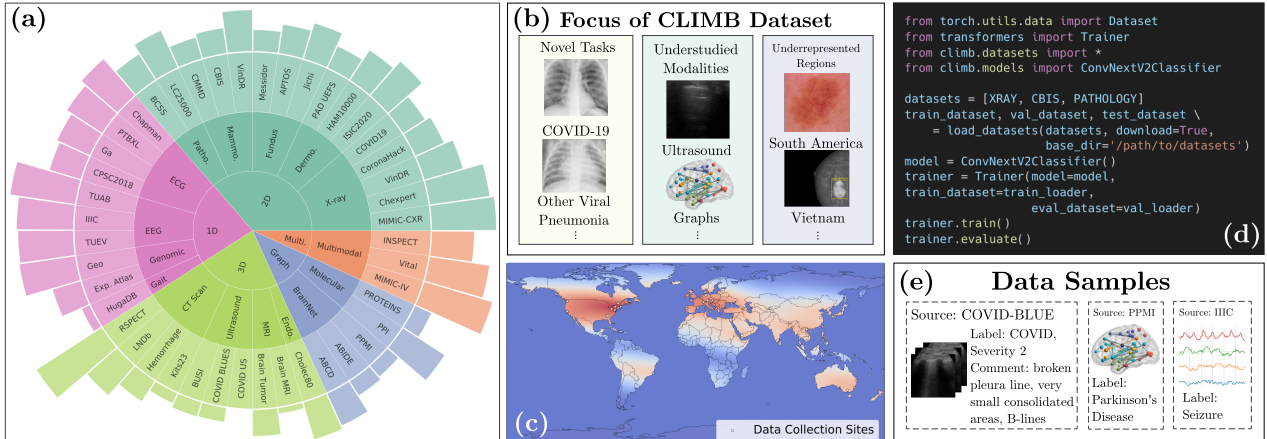
Figure 2. **Overview of CLIMB benchmark and code. (a) Visualization of CLIMB dataset composition.** The inner ring displays the primary data modalities (2D, 1D, Graph, Multimodal). The middle ring represents major clinical modalities within each modality. The outer ring shows the names of specific datasets within each category, with the outer bar plot representing the number of samples in that dataset. A detailed description of each modality and datasets are included in App. A. **(b) Focus of dataset collection.** During the collection of CLIMB, we aim to collect a diverse range of datasets, with a special focus on novel tasks, datasets from understudied modalities, and datasets from underrepresented regions. **(c) Distribution of data collection sites in CLIMB.** Red regions indicate areas where clinical datasets are commonly collected, whereas blue regions indicate places where clinical dataset collections are rare. **(d) Example code usage on CLIMB framework.** This code example loads a custom mixed subset of CLIMB spanning across three modalities, then trains a ConvNextv2 classifier on the dataset mixture with unified vocabulary. **(e) Sample data from CLIMB.** CLIMB preserves detailed labels, metadata and comments explaining the diagnosis.

tasks, but notably do not optimize the visual components. In contrast, vision-focused works like Swin-Unet (Cao et al., 2022) develop specialized encoders for clinical imaging, though typically for single modalities. M4oE (Jiang & Shen, 2024) represents a rare exception, using Swin Transformers (Liu et al., 2021) to create a mixture of experts model across both CT and MRI modalities, but they failed to expand it further into more modalities. While general vision architectures like ConvNeXt and EVA-2 (Liu et al., 2022; Fang et al., 2024) have demonstrated strong performance on natural images, efforts to develop clinical-specific encoders have largely focused on adapting older architectures, as seen in CLIP-based PMC-CLIP (Lin et al., 2023) and Vision Transformer-based MedViT (Manzari et al., 2023), leaving the potential of modern architectures for clinical tasks largely unexplored.

3. Dataset

In this section, we provide an overview of the CLIMB dataset, sourced from 44 public datasets spanning 15 modalities in 13 clinical domains. A detailed description of each modality and dataset is included in App. A. We first introduce the selection criteria of the CLIMB dataset, followed by the dataset information and statistics. In the end, we provide a simple code snippet demonstrating the use of CLIMB for model training and inference.

3.1. Dataset Selection Criteria

CLIMB unifies diverse public clinical datasets into a unified benchmark designed specifically for developing and evaluating multimodal medical AI systems. To maximize the diversity of the data, we established three key criteria to guide our dataset selection process. As illustrated in Figure 2(b), we prioritize datasets that address one or more of the following objectives:

1. **Novel tasks:** Recent emerging clinical challenges, such as COVID-19 diagnosis from chest imaging.
2. **Understudied modalities:** Data types traditionally underrepresented in clinical AI, including electroencephalograms (EEG), endoscopic videos, and graphs.
3. **Underrepresented regions:** Clinical data from geographic areas with limited representation in existing benchmarks, particularly South America and developing regions of South Asia.

A detailed description of our selection methodology and inclusion criteria is provided in App. A.2.

3.2. Dataset Construction

Based on the selection criteria above, CLIMB was eventually sourced from 44 public datasets. Fig. 2(e) shows three examples in CLIMB, with labels COVID-19, Parkinson's disease and Seizure, from ultrasound, brain network, and EEG, respectively (Wie, 2021; Cui et al., 2022; Jing et al., 2023a). Notably, additional metadata and explanation labels for the datasets are also preserved, as shown in the

Table 1. **Comparison of clinical benchmarks.** Abbreviations: BN = Brain Networks, Mol = Molecules, ECG = Electrocardiogram, EEG = Electroencephalogram, Genom = Genomics, Mammo = Mammography, Derm = Dermoscopy, Fund = Fundus, Path = Pathology, CT = Computed Tomography, MRI = Magnetic Resonance Imaging, US = Ultrasound, Endo = Endoscopy. CLIMB (ours) is the the most diverse, comprehensive, largest clinical public multimodal dataset up to date, which enables holistic studies on multiple modalities and provides data foundation for large-scale clinical pretraining across vision, language, time series and graphs. * For BenchMD, 5.1M out of 5.2M samples are EEGs, with only 0.1M samples from other modalities.

Dataset	#Samples	Graph		1D					2D					3D			
		BN	Mol	ECG	EEG	Genom	Gait	Text	X-ray	Mammo	Derm	Fund	Path	CT	MRI	US	Endo
BenchMD (Wantlin et al., 2023)	5.2M*	✗	✗	✓	✓	✗	✗	✗	✓	✓	✓	✓	✗	✓	✗	✗	✗
PMC-VQA (Zhang et al., 2023)	149K	✗	✗	✗	✗	✗	✗	✓	✓	✗	✗	✗	✗	✓	✓	✓	✗
GMAI-MMBench (Chen et al., 2024)	26K	✗	✗	✗	✗	✗	✗	✓	✓	✗	✓	✓	✗	✓	✓	✓	✓
CARES (Xia et al., 2024)	18K	✗	✗	✗	✗	✗	✗	✓	✓	✗	✓	✓	✓	✓	✓	✓	✓
CLIMB (ours)	4.51M	✓	✓	✓	✓	✓	✓	✓	✓	✓	✓	✓	✓	✓	✓	✓	✓

COVID-19 ultrasound example.

To enable holistic training and benchmarking, we need to unify the input data loading and prediction tasks. To unify the label space, we consider two options. The first is to pose all tasks as multi-label classification given clinical data samples from different modalities. We combine the vocabularies in each dataset while merging semantically equivalent labels. Specifically, given a heterogeneous dataset collection $\mathcal{D} = \{D_1, ..., D_K\}$ with mixed annotation types (multi-label/multi-class), we define a unified label vocabulary $\mathcal{V} = \bigcup_{k=1}^{K} V_k$ where V_k represents the label set of dataset D_k. To ensure consistency, we standardize terminology variations and combine similar concepts such as *Lung Opacity* from Chexpert and *Infiltration* from Vindr CXR to maintain a clean, unified vocabulary while preserving the original clinical meaning. The list of classes are included in App. Table 7.

The second option is to pose everything as QA. We also built a closed choice question-answering version of the dataset, namely CLIMB-QA, for comparable LVLM evaluation. In CLIMB-QA, each dataset is preprocessed with QA pairs containing close-ended multiple-choice questions. A detailed description of CLIMB-QA along with examples are included in App. B.

In addition, we preserve the metadata, demographic information, segmentation masks, and associated clinical reports from the original dataset and link them to every sample where applicable. To ensure comparability across model architectures, this information is not exposed to the model in the experiments, although we hope future works could utilize it to develop more robust and fair methods.

3.3. Dataset Statistics

CLIMB contains 4.51 million samples totaling 19.01 terabytes, with the following composition: 871K (19.31%) 1D time series and text data (including electronic health records, EEG, ECG, gait and genomic data), 707K (15.68%) 2D images (including X-rays, dermoscopy images, fundus images, and pathology slides), 1.83M (40.56%) 3D or video data (including ultrasounds, CT scans, endoscopic images and MRI images), 69.3K (1.54%) graph data (including brain networks, molecules), and 1.03M (22.90%) multimodality data combining multiple of the above modalities. As shown in Table 1, CLIMB has the widest range of modalities while incorporating time series and graph data, which distinguishes it from existing multimodal benchmarks in the field that typically only include images and text.

Figure 2(a) shows the distribution across primary modalities and the size of individual datasets. We carefully balance the dataset such that each modality contains 3-5 datasets, providing multiple data sources per modality while maintaining diversity within each category.

The geographic distribution of data sources is shown in Figure 2(c). The dataset includes data from 37 medical institutions across 18 countries, including contributions from Vietnam, Iraq, India, and Brazil, expanding the representation beyond traditionally well-represented regions.

3.4. Dataset Interface and Code Usage

We present a unified interface to download and process our dataset into a unified format for mixed large-scale pretraining, given that the user has provided agreement consents on individual dataset websites. Figure 2(d) shows the code for a standard workflow of loading multiple medical imaging datasets and training a classification model with our CLIMB framework. The entire training and evaluation script can be completed in under ten lines of code while maintaining the flexibility for any custom models or training loops. We also provide a standardized training pipeline that is easily reproducible and parallelizable across multiple machines and instances.

4. Experiments

We run extensive experiments to investigate the core technical challenges for developing clinical foundation models with CLIMB. Specifically, we ask the following questions:
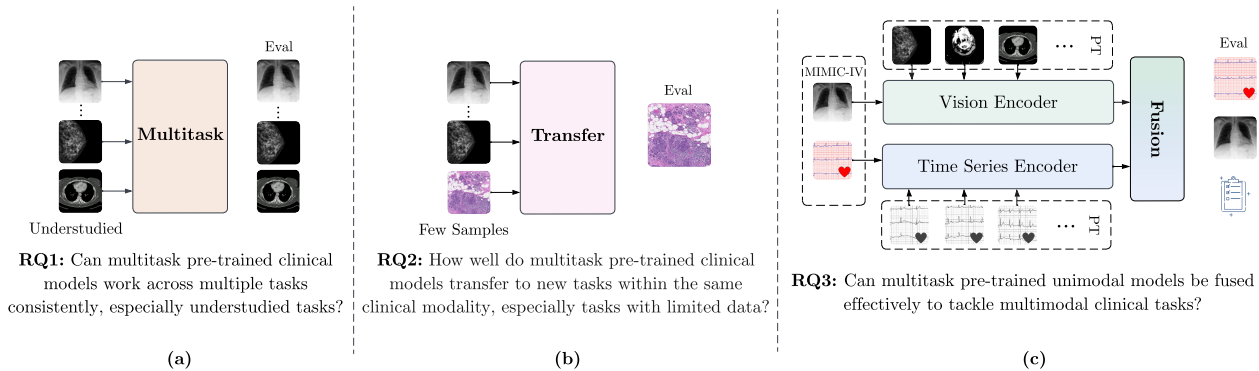
Figure 3. **Experimental setup for evaluating (a) multitask, (b) transfer, and (c) fusion learning strategies, addressing RQ1, 2, 3 respectively.** (a) investigates how multitask pretrained clinical models work across multiple tasks consistently, especially understudied tasks. (b) explores how well multitask pretrained clinical models transfer to new tasks with few samples within the same clinical modality. (c) experiments on whether multitask pretrained unimodal models can be fused effectively to tackle multimodal clinical tasks.

1. **RQ1:** Can multitask pretrained clinical models work across multiple tasks consistently, especially for under-studied tasks?
2. **RQ2:** How well do multitask pretrained clinical models transfer to new tasks within the same clinical modality, especially tasks with limited data?
3. **RQ3:** Can multitask pretrained unimodal models be fused effectively to tackle multimodal clinical tasks?

4.1. Experimental setup

To answer the above research questions, we design our experiments as follows:

RQ1: Multitask pretraining. We investigate whether multitask learning can enable robust universal encoders for clinical tasks. For each input modality (vision 2D/3D, graph, EEG, ECG), we train a single encoder jointly on all related tasks in CLIMB. Each encoder is combined with a classification head that predicts task-specific labels from an aggregated vocabulary $\mathcal{V}$, which encompasses diagnostic terms across all tasks within that modality. For each modality, we evaluate both specialized medical models and general-domain architectures. In vision, we compare medical-specific encoders (MedViT (Manzari et al., 2023), PMC-CLIP (Lin et al., 2023), RAD-DINO (Pérez-García et al., 2025)) against general vision models (ConvNeXTv2 (Liu et al., 2022), SBB2 (Radford et al., 2021), Swin Transformer (Liu et al., 2021), EVA-2 (Fang et al., 2024), Intern-ViT (Chen et al., 2023)). For time-series data, we evaluate ECG-specific model, ECG JEPA (Kim, 2024), against general time-series architectures, UniTS (Gao et al., 2024). In the EEG domain, we test specialized architectures including SPARCNet (Jing et al., 2023b), CNNTransformer (Peh et al., 2022), FFCL (Li et al., 2022), ContraWR (Yang et al., 2021), STTransformer (Song et al., 2021), and BIOT (Yang et al., 2024). We also evaluate SoTA clinical VLM, LLaVa-Med (Li et al., 2023), on CLIMB-QA, a question-answering

version of CLIMB designed for comparability across large VLMs and traditional encoders. Details on construction are included in App. B.

RQ2: Few-shot transfer. We investigate how well models pretrained on CLIMB can generalize to novel clinical tasks with limited labeled data. To evaluate few-shot generalization, we test on out-of-distribution (OOD) datasets $\mathcal{D}_{ood} \not\subset \mathcal{D}_{train}$. The OOD datasets are selected to reflect either a new task or a different data source within the same modality, simulating real-world scenarios where models must adapt to novel diagnostic tasks with limited labeled examples (1, 8, and 32 samples). We curated a diverse set of 10 datasets spanning 9 modalities, as detailed in App. C.7.1. For each modality, we use the best-performing model from our RQ1 experiments: ConvNextv2 for vision tasks, ECG JEPA for ECG analysis, and BIOT for EEG processing. We compare two scenarios: (1) models initialized with publicly released pretrained weights, and (2) models pretrained on CLIMB. Both are then fine-tuned using few-shot samples from the target OOD dataset.

RQ3: Unimodal pretraining to multimodal fusion. We investigate how to effectively combine information from different clinical modalities (imaging, text, and time series) to improve patient outcome prediction. This addresses the practical clinical scenario where multiple types of medical data are available for diagnosis and prognosis. Our experiments pretrain models on CLIMB and transfer them to MIMIC-IV (Johnson et al., 2023), a large-scale multimodal clinical dataset. We evaluate three fusion strategies with increasing levels of cross-modal interaction: Late fusion, MLP fusion, and cross-attention fusion. Detailed architectural specifications are provided in App. C.2.3. We fix the encoder architectures across all experiments: ConvNextv2 for visual inputs, ClinicalBERT for text, and ECG-JEPA for time series data. In addition, to evaluate how large scale pretraining helps with multimodal tasks across dif-

Table 2. **Performance comparison of trained multitask models across various medical imaging modalities.** Sen: Sensitivity, Spe: Specificity, AUC: Area under the receiver operating characteristic curve. CLIP-L2B: CLIP ViT-Laion 2B. The best performance of each model in AUC is bolded. Detailed breakdowns of each dataset are attached in App. D.1. The experiment shows that general domain SoTA encoders perform better than specialized medical encoders, with ConvNeXTv2 offering the best performance-compute tradeoff.

Model	Chest X-Ray			Mammography			Dermoscopy			CT Scan			Fundus			Ultrasound			Overall		
	AUC	Sen	Spe	AUC	Sen	Spe	AUC	Sen	Spe	AUC	Sen	Spe	AUC	Sen	Spe	AUC	Sen	Spe	AUC	Sen	Spe
Clinical Encoders																					
MedViT	.670	.253	.833	.627	.417	.583	.522	.361	.639	.604	.382	.616	.320	.317	.688	.452	.500	.583	.579	.364	.690
PMC-CLIP	.725	.251	.883	.614	.312	.710	.674	.325	.706	.619	.407	.593	.508	.220	.785	.521	.384	.609	.635	.341	.724
RAD-DINO	.818	.406	.928	.566	.314	.701	.717	.348	.715	.653	.408	.594	.606	.221	.786	.639	.431	.619	.681	.368	.729
General Domain Encoders																					
SBB2	.791	.401	.922	.538	.262	.663	.784	.362	.724	.691	.403	.590	.732	.293	.821	.711	.495	.689	.730	.420	.754
Swin Transformer	.795	.389	.926	.513	.200	.599	.815	.435	.747	.685	.429	.615	.770	.327	.838	.705	.545	.712	.765	.436	.775
EVA-2	**.863**	.382	.929	.516	.320	.699	.716	.353	.724	.531	**.496**	.496	.780	.295	.822	.462	.340	.659	.685	.372	.737
InternViT	.815	.413	.930	.532	**.340**	**.713**	.868	.543	.770	**.706**	.469	**.652**	.839	.431	.851	.735	.549	.718	.772	.492	.789
ConvNeXTv2	.817	**.436**	**.939**	**.558**	.330	.706	**.901**	**.568**	**.777**	.671	.466	.641	**.873**	**.563**	**.888**	**.774**	**.641**	**.770**	**.787**	**.537**	**.806**

Table 3. **Performance comparison of graph neural networks across brain networks and protein structures.** The best performance of each model is bolded. Graph transformer offers the best performance in terms of AUC and sensitivity-specificity balance.

Model	BrainNet			Molecular			Overall		
	AUC	Sen	Spe	AUC	Sen	Spe	AUC	Sen	Spe
GCN	.804	.696	.800	.763	.532	.760	.783	.614	.780
GAT	.705	**.916**	.404	**.823**	**.551**	.801	.764	**.733**	.602
Graph Transformer	**.852**	.810	**.826**	.789	.381	**.920**	**.820**	.595	**.873**

ferent encoders, we compare models initialized with our CLIMB pretrained weights against those using publicly available pretrained weights. We evaluate on two common clinical prediction tasks: length of stay (LOS) prediction and 48-hour in-hospital mortality prediction (48 IHM). These tasks are clinically significant and require integrating information across modalities.

Evaluation metrics. For consistency, we evaluate all classification tasks with balanced AUC, sensitivity, and specificity. Regression tasks (e.g., length of stay prediction) are evaluated with mean absolute error (MAE). Task specifications, metrics considerations and experimental setups are provided in App. C.

4.2. On RQ1: Multitask Pretraining Performance

Importance of multitask pretraining. Our experiments demonstrate that multitask pretraining yields substantial and consistent improvements across diverse clinical scenarios, as shown in Fig. 4. Notably, the most significant gains are observed in the three understudied categories: novel tasks, understudied modalities, and datasets from underrepresented regions, as detailed in Sec. 3.1. Datasets that intersect multiple categories show the highest performance improvements, as exemplified by COVID-US with an AUC gain of 0.3254. In temporal modalities, particularly ECG analysis, the Ga dataset demonstrates this trend with an absolute AUC improvement of 23 percentage points (from
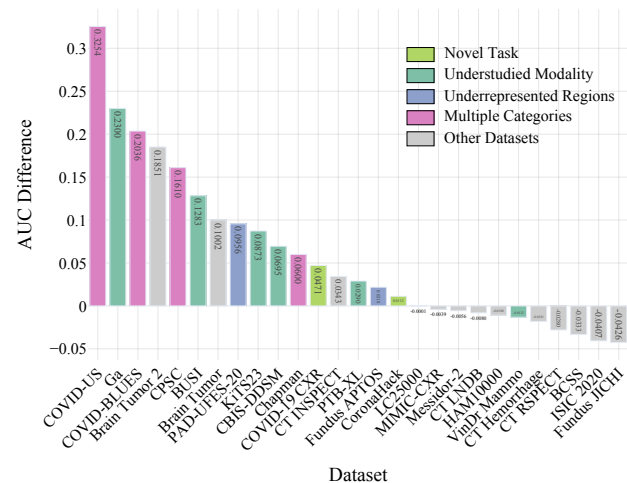

Figure 4. **Difference in AUC achieved by the multitask model compared to single-task training.** Novel Task represent emerging clinical challenges like COVID-19; Underrepresented Regions indicates datasets from underrepresented regions in developing countries such as Brazil and China; Understudied Modalities includes less common imaging types such as ultrasound and CT scans. Datasets belonging to multiple categories are highlighted in pink. In general, multitask learning helps the model to reach a better performance, with the greatest improvement observed in understudied tasks, regions, and/or modalities.

0.474 to 0.704) when comparing single-task to multitask pretraining approaches, as shown in Table D.1. These results suggest that multitask learning is particularly effective for scenarios where data or research attention has been historically limited.

Comparison of encoder models. Our analysis reveals counterintuitive patterns in encoder effectiveness across different domains. In the visual domain, image-based models consistently outperform video models across both image and video tasks, which we attribute to the substantially larger pretraining datasets available for image models. In

Table 4. **Performance comparison of zero-shot and fine-tuned LLaVa-Med.** LLaVa-Med is the current SoTA LVLM model for clinical QA tasks. Both CLIMB-ConvNextv2 and LLaVa-Med are trained and evaluated on CLIMB in a comparable, close-ended manner. While directly fine-tuning the LLM on CLIMB-QA improves performance over zero-shot cases, they still lag behind SoTA multitask encoders, namely CLIMB-ConvNextv2, the SoTA multitask encoder trained on CLIMB.

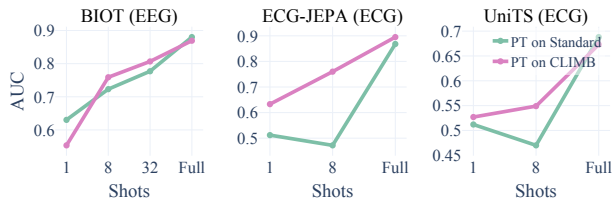| Dataset	Zero-Shot			Fine-Tuned		
	Acc	Sens	Spe	Acc	Sens	Spe
Chest X-ray	.088	.192	.808	.309	.207	.795
MRI	.363	.473	.650	.480	.375	.625
Ultrasound	.448	.427	.640	.579	.389	.611
Mammography	.049	.203	.800	.741	.300	.700
Dermoscopy	.466	.296	.700	.673	.245	.756
Fundus	.434	.202	.794	.578	.217	.783
CT	.448	.424	.575	.788	.435	.585
Endoscopic	.000	1.00	.000	.296	.143	.857
Average	.287	.402	.621	.555	.289	.714
CLIMB-ConvNextv2	-	-	-	**.877**	**.806**	**.787**

Figure 5. **Few-shot learning performance comparison across different time series domains.** We evaluate the few-shot performance (1-shot, 8-shot, and full dataset) of three representative models: BIOT for EEGs, ECG-JEPA and UniTS for ECGs. PT on Standard shows the performance when pretrained on their datasets from the original paper, while PT on CLIMB shows the performance when pretrained on our CLIMB dataset. Models pretrained on CLIMB demonstrate consistent improvements over the original ECG domain-specific models.

addition, general-purpose architectures like ConvNextv2 significantly outperform clinical-specific encoders such as MedViT, achieving a 35.9% performance improvement. We hypothesize this superiority stems from the more diverse pretraining distribution encountered by general-domain encoders. However, in the ECG domain, specialized architectures demonstrate clear advantages, with ECG JEPA outperforming the general-purpose time series model UniTS by 36.8%. This dichotomy suggests that the optimal choice of architecture depends heavily on both the modality and the availability of domain-specific pretraining data. In the graph domain, graph transformers work the best with the highest score across all metrics, as shown in Tab. 3.

Comparing Vision Encoders with Large VLMs. We evaluated LLaVa-Med on CLIMB-QA to assess current clinical VLMs' capabilities in multimodal understanding. While fine-tuning on CLIMB-QA improves performance over zero-
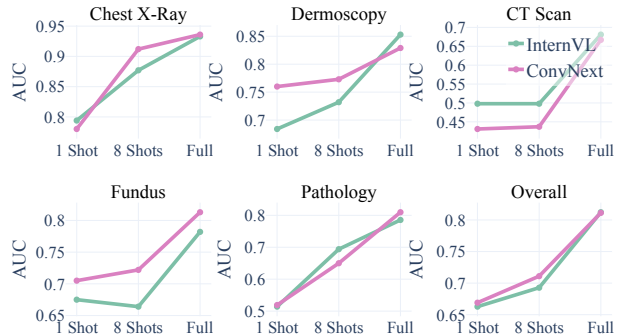

Figure 6. **Few-shot performance on out-of-distribution datasets.** InternVL represents the ViT-based model, while ConvNext represents the convolution-based model. In general, ViT-based models and ConvNext-based models exhibit similar overall performances across all shots, with ViT excelling at CT Scan tasks while ConvNext performs better at diagnosing fundus images.

shot inference by 28.7% percentage points, these results significantly lag behind CLIMB-ConvNextv2, our new SoTA vision encoder trained on CLIMB, by 32.2% percentage points in accuracy. The gap is particularly evident in modalities requiring fine-grained visual understanding, such as chest X-rays (0.309 accuracy) and endoscopic images (0.296 accuracy), where the model struggles to maintain balanced sensitivity and specificity. These results suggest that CLIMB is a rich data source of clinical AI that can substantially improve existing models and that current vision-language models still require fundamental architectural innovations and novel training paradigms.

4.3. On RQ2: Few-shot Transfer Performance

Strength of few-shot transfer. As illustrated in Figure 7, our large-scale pretraining dataset enables efficient learning of novel tasks with limited samples, demonstrating consistent performance improvements across all modalities. The impact is particularly significant in traditionally challenging modalities such as CT scans and ultrasound imaging, where models achieved substantial gains in AUC of 28.7% and 29.1%, respectively. In time series domains such as ECG and EEG, our model outperformed SoTA weights specifically trained on this domain, which again illustrates the benefits of our large-scale pertaining data.

Architecture comparisons. As shown in Figure 6, in the vision domain, we again found both ConvNextv2 and ViT-based models perform similarly under both full and few shot settings, as shown in Figure 6. ConvNext exhibit better performance in fundus and dermoscopy images, while ViT performs better for CT scans. We also found specialized ECG models like ECG-JEPA transfer better than universal time series models like UniTS, as demonstrated in Figure 5.
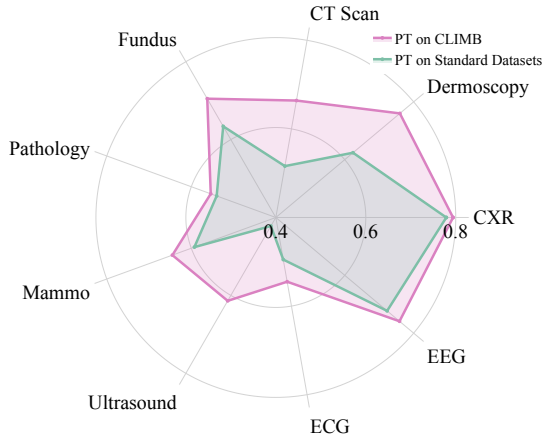
Figure 7. **Few-shot performance of models across different pre-training (PT) datasets.** CXR: Chest X-ray. We use ConvNextv2 for vision, ECG JEPA for ECG data, and BIOT for EEGs. PT on Standard Datasets is the performance of training one shot example on top of their own pretrained weights, while PT on CLIMB is the performance of training one shot example on top of our CLIMB dataset. For EEGs, 8 shot results are used instead due to the inherent complexity of the task.

4.4. RQ3: Unimodal Pretraining to Multimodal Fusion Pretraining results.

Experimental results in Table 5 demonstrate that encoders pretrained on CLIMB consistently outperform those pretrained on other datasets across all evaluation settings. This performance advantage is maintained across diverse tasks, including length of stay prediction and in-hospital mortality prediction, both in full-data and few-shot scenarios. Notably, our pretrained encoders achieve 5.78% lower MAE (2.61 vs 2.77) in LOS prediction and 15.9% higher AUC in 8-shot mortality prediction, suggesting that the diverse modalities in CLIMB enable more robust feature representations.

Fusion comparisons. Our analysis reveals that the effectiveness of different fusion strategies varies with task complexity. For complex regression tasks like length of stay prediction, cross-attention mechanisms demonstrate superior performance, achieving the lowest MAE of 2.61. In contrast, for binary classification tasks such as 48-hour in-hospital-mortality (48 IHM) prediction, MLP-based concatenation proves more effective, achieving the highest AUC while maintaining balanced sensitivity (0.824) and specificity (0.975). While late fusion appears to achieve higher specificity in some cases, its near-zero sensitivity indicates that it effectively defaults to predicting the majority class without any meaningful information. This pattern persists in the challenging 8-shot setting, where MLP fusion maintains the best performance while preserving a reasonable balance between sensitivity and specificity.

Table 5. **Performance comparison of different multimodal fusion approaches on length of stay (LOS) prediction and 48-hour in-hospital mortality (48 IHM) prediction tasks.** CrossAtt: Cross Attention. Unimodal encoders trained on CLIMB transfers to better multimodal performance, given proper fusion strategies are used. Complex tasks like LOS require complex fusions like cross-attention, while simple tasks like 48 IHM work well under simple MLP fusion.

Enc.	Fusion	LOS	48 IHM (Full)			48 IHM (8-Shots)		
		MAE	AUC	Sens	Spec	AUC	Sens	Spec
SoTA	**Late**	4.78	0.689	0.495	0.760	0.524	0.001	**0.994**
	MLP	2.98	0.957	0.806	0.979	0.556	0.536	0.538
	CrossAtt	2.77	0.786	0.628	0.814	0.580	0.286	0.766
Ours	**Late**	4.71	0.859	0.017	**0.983**	0.628	0.022	0.993
	MLP	2.84	**0.961**	**0.824**	0.975	**0.672**	**0.295**	0.858
	CrossAtt	**2.61**	0.796	0.822	0.590	0.570	0.294	0.753

4.5. Comparison with Dataset-Specific SoTAs

To contextualize the performance of our pretrained unimodal and multimodal models, we compare them to prior reported results from state-of-the-art models specifically optimized for individual datasets in App. Table 29. While dataset-specific architectures sometimes outperform pretrained models through specialized optimizations, they often struggle to adapt to new tasks, even within the same modality it was trained on (see Sec. 4.2). The highly specialized nature of their architectures, like the multi-stage category-wise fine-tuning utilized in CFT (Chong et al., 2023), makes them difficult to adapt or retrain for different clinical tasks. Therefore, there is much value in training generalizable unimodal and multimodal models that can effectively adapt across diverse clinical modalities, tasks, and scenarios.

5. Conclusion

We present CLIMB, a comprehensive multimodal clinical benchmark unifying 4.51M samples across 44 datasets, 15 modalities, and 13 clinical domains. Our extensive empirical evaluation revealed several key insights for clinical AI development. First, multitask pretraining significantly improves performance on understudied modalities and novel tasks. Second, general-domain architectures outperform clinical-specific ones in multitask settings. Third, models pretrained on CLIMB demonstrate substantial improvements in few-shot scenarios across modalities. Finally, unimodal pretraining on CLIMB consistently enhances performance on downstream multimodal tasks. Based on these findings, we recommend leveraging general-domain architectures for visual tasks and emphasize the importance of multitask pretraining, especially for understudied domains. For multimodal applications, we suggest matching fusion complexity to task requirements and utilizing large-scale unimodal pretraining before multimodal integration.

Looking ahead, our findings point to several emerging re-

search directions: developing novel architectures that better balance general and domain-specific features, finding new ways to combine unexplored modality combinations, and creating fusion mechanisms that adjust to task complexity. While dataset-specific models currently achieve higher performance through specialized optimizations, we encourage future research to develop general multitask encoders that can effectively adapt across diverse modalities and tasks. By releasing our dataset, code, and models, we hope to accelerate progress in these directions and advance the development of holistic clinical AI systems.

Impact Statement

This paper presents empirical benchmarking, analysis, and development of multimodal clinical datasets and models. Multimodal AI can help clinicians analyze large-scale longitudinal data, make predictions, and investigate interventions. Furthermore, increasingly many indicators are no longer taken in the doctor's office, but daily, such as physiological sensors that track sleep, mood, stress, diet, exercise, and social interactions. Our findings can have a broad impact on developing holistic AI models of human health and wellness.

At the same time, data privacy and model fairness are critical qualities. There may be privacy risks associated with collecting and making predictions from multimodal clinical data. We have taken appropriate steps to only access data that participants have consented to public release, and to the best of our knowledge, all data was anonymized and stripped of all personal (e.g., personally identifiable information) and protected attributes (e.g., race, gender). There is also the risk that clinical AI models capture spurious features from race, gender, and other demographic variables, especially as more clinical data is provided. To deploy these algorithms at scale in the real world, it is also important to keep data and features secure without public sharing.

Overall, CLIMB offers opportunities to study the promises of multimodal AI while mitigating potential risks at scale across clinical modalities, tasks, and domains. We will continue expanding CLIMB to rigorously test for these social impacts and improve the safety and reliability of multimodal clinical models. Our holistic evaluation metrics will also encourage the research community to quantify the tradeoffs between performance, complexity, robustness, fairness, and privacy in clinical AI.

References

Abràmoff, M. D., Folk, J. C., Han, D. P., Walker, J. D., Williams, D. F., Russell, S. R., Massin, P., Cochener, B., Gain, P., Tang, L., Lamard, M., Moga, D. C., Quellec, G., and Niemeijer, M. Automated analysis of retinal images for detection of referable diabetic retinopathy. *JAMA Ophthalmology*, 131(3):351–357, 2013. doi: 10.1001/jamaophthalmol.2013.1743. URL https://doi.org/10.1001/jamaophthalmol.2013.1743.

Al-Dhabyani, W., Gomaa, M., Khaled, H., and Fahmy, A. Dataset of breast ultrasound images. *Data in brief*, 28:104863, 2020.

Alday, E. A. P., Gu, A., Shah, A. J., Robichaux, C., Wong, A.-K. I., Liu, C., Liu, F., Rad, A. B., Elola, A., Seyedi, S., et al. Classification of 12-lead ecgs: the physionet/computing in cardiology challenge 2020. *Physiological measurement*, 41(12):124003, 2020.

Asia Pacific Tele-Ophthalmology Society. APTOS 2019 blindness detection. https://www.kaggle.com/c/aptos2019-blindness-detection/data, 2019. [Dataset].

Bhuvaji, S., Kadam, A., Bhumkar, P., Dedge, S., and Kanchan, S. Brain tumor classification (mri), 2020. URL https://www.kaggle.com/dsv/1183165.

Borgwardt, K. M., Ong, C. S., Schönauer, S., Vishwanathan, S., Smola, A. J., and Kriegel, H.-P. Protein function prediction via graph kernels. *Bioinformatics*, 21(suppl_1):i47–i56, 2005.

Borkowski, A. A., Bui, M. M., Thomas, L. B., Wilson, C. P., DeLand, L. A., and Mastorides, S. M. Lung and colon cancer histopathological image dataset (lc25000). *arXiv preprint arXiv:1912.12142*, 2019.

Cao, H., Wang, Y., Chen, J., Jiang, D., Zhang, X., Tian, Q., and Wang, M. Swin-unet: Unet-like pure transformer for medical image segmentation. In Karlinsky, L., Michaeli, T., and Nishino, K. (eds.), *Computer Vision - ECCV 2022 Workshops - Tel Aviv, Israel, October 23-27, 2022, Proceedings, Part III*, volume 13803 of *Lecture Notes in Computer Science*, pp. 205–218. Springer, 2022. doi: 10.1007/978-3-031-25066-8_9. URL https://doi.org/10.1007/978-3-031-25066-8_9.

Chen, P., Ye, J., Wang, G., Li, Y., Deng, Z., Li, W., Li, T., Duan, H., Huang, Z., Su, Y., Wang, B., Zhang, S., Fu, B., Cai, J., Zhuang, B., Seibel, E. J., He, J., and Qiao, Y. Gmai-mmbench: A comprehensive multimodal evaluation benchmark towards general medical ai. *arXiv preprint:2408.03361*, 2024. URL https://doi.org/10.48550/arXiv.2408.03361.

Chen, Z., Wu, J., Wang, W., Su, W., Chen, G., Xing, S., Zhong, M., Zhang, Q., Zhu, X., Lu, L., Li, B., Luo, P., Lu, T., Qiao, Y., and Dai, J. Internvl: Scaling up vision foundation models and aligning for generic visual-linguistic tasks. *CoRR*, abs/2312.14238, 2023. doi: 10.48550/ARXIV.2312.14238. URL https://doi.org/10.48550/arXiv.2312.14238.

Chereshnev, R. and Kertész-Farkas, A. Hugadb: Human gait database for activity recognition from wearable inertial sensor networks. In *Analysis of Images, Social Networks and Texts: 6th International Conference, AIST 2017, Moscow, Russia, July 27–29, 2017, Revised Selected Papers 6*, pp. 131–141. Springer, 2018.

Chong, C. F., Yang, X., Wang, T., Ke, W., and Wang, Y. Category-wise fine-tuning for image multi-label classification with partial labels. In *International Conference on Neural Information Processing*, pp. 332–345. Springer, 2023.

Cohen, J. P., Morrison, P., and Dao, L. Covid-19 image data collection. *arXiv 2003.11597*, 2020. URL https://github.com/ieee8023/covid-chestxray-dataset.

Colak, E., Kitamura, F. C., Hobbs, S. B., Wu, C. C., Lungren, M. P., Prevedello, L. M., Kalpathy-Cramer, J., Ball, R. L., Shih,

G., Stein, A., et al. The rsna pulmonary embolism ct dataset. *Radiology: Artificial Intelligence*, 3(2):e200254, 2021.

Cui, C., Li, L., Cai, H., Fan, Z., Zhang, L., Dan, T., Li, J., and Wang, J. The chinese mammography database (cmmd): An online mammography database with biopsy confirmed types for machine diagnosis of breast. *The Cancer Imaging Archive*, 2021. doi: 10.7937/TCIA.EQDE-4B16. URL https://doi.org/10.7937/tcia.eqde-4b16.

Cui, H., Dai, W., Zhu, Y., Kan, X., Gu, A. A. C., Lukemire, J., Zhan, L., He, L., Guo, Y., and Yang, C. Braingb: a benchmark for brain network analysis with graph neural networks. *IEEE transactions on medical imaging*, 42(2):493–506, 2022.

Cui, H., Mao, L., Liang, X., Zhang, J., Ren, H., Li, Q., Li, X., and Yang, C. Biomedical visual instruction tuning with clinician preference alignment. *arXiv preprint arXiv:2406.13173*, 2024.

Decencière, E., LaGraize, C., Pélégrin, P., Benassi, F., Régér, C., and Vautrin, T. Feedback on a publicly distributed database: the messidor database. *Image Analysis & Stereology*, 33(3): 231–234, 2014. ISSN 1854-5165. doi: 10.5566/ias.1155. URL http://dx.doi.org/10.5566/ias.1155.

Diederik, P. K. Adam: A method for stochastic optimization. *(No Title)*, 2014.

Ebadi, A., Xi, P., MacLean, A., Tremblay, S., Kohli, S., and Wong, A. Covidx-us–an open-access benchmark dataset of ultrasound imaging data for ai-driven covid-19 analytics. *arXiv preprint arXiv:2103.10003*, 2021.

Esteva, A., Robicquet, A., Ramsundar, B., Kuleshov, V., DePristo, M., Chou, K., Cui, C., Corrado, G., Thrun, S., and Dean, J. A guide to deep learning in healthcare. *Nature medicine*, 25(1): 24–29, 2019.

Fang, Y., Sun, Q., Wang, X., Huang, T., Wang, X., and Cao, Y. EVA-02: A visual representation for neon genesis. *Image Vis. Comput.*, 149:105171, 2024. doi: 10.1016/J.IMAVIS.2024. 105171. URL https://doi.org/10.1016/j.imavis.2024.105171.

Gao, S., Koker, T., Queen, O., Hartvigsen, T., Tsiligkaridis, T., and Zitnik, M. Units: A unified multi-task time series model, 2024. URL https://arxiv.org/abs/2403.00131.

Goldberger, A. L., Amaral, L. A., Glass, L., Hausdorff, J. M., Ivanov, P. C., Mark, R. G., Mietus, J. E., Moody, G. B., Peng, C.-K., and Stanley, H. E. Physiobank, physiotoolkit, and physionet: components of a new research resource for complex physiologic signals. *circulation*, 101(23):e215–e220, 2000.

Heller, N., Isensee, F., Trofimova, D., Tejpaul, R., Zhao, Z., Chen, H., Wang, L., Golts, A., Khapun, D., Shats, D., et al. The kits21 challenge: Automatic segmentation of kidneys, renal tumors, and renal cysts in corticomedullary-phase ct. *arXiv preprint arXiv:2307.01984*, 2023.

Hssayeni, M., Croock, M., Salman, A., Al-khafaji, H., Yahya, Z., and Ghoraani, B. Computed tomography images for intracranial hemorrhage detection and segmentation. *Intracranial hemorrhage segmentation using a deep convolutional model. Data*, 5 (1):14, 2020.

Huang, K., Altosaar, J., and Ranganath, R. Clinicalbert: Modeling clinical notes and predicting hospital readmission. *arXiv preprint arXiv:1904.05342*, 2019.

Huang, S.-C., Huo, Z., Steinberg, E., Chiang, C.-C., Lungren, M. P., Langlotz, C. P., Yeung, S., Shah, N. H., and Fries, J. A. Inspect: a multimodal dataset for pulmonary embolism diagnosis and prognosis. *arXiv preprint arXiv:2311.10798*, 2023.

Irvin, J., Rajpurkar, P., Ko, M., Yu, Y., Ciurea-Ilcus, S., Chute, C., Marklund, H., Haghgoo, B., Ball, R., Shpanskaya, K., et al. Chexpert: A large chest radiograph dataset with uncertainty labels and expert comparison. In *Proceedings of the AAAI conference on artificial intelligence*, volume 33, pp. 590–597, 2019a.

Irvin, J., Rajpurkar, P., Ko, M., Yu, Y., Ciurea-Ilcus, S., Chute, C., Marklund, H., Haghgoo, B., Ball, R. L., Shpanskaya, K. S., Seekins, J., Mong, D. A., Halabi, S. S., Sandberg, J. K., Jones, R., Larson, D. B., Langlotz, C. P., Patel, B. N., Lungren, M. P., and Ng, A. Y. Chexpert: A large chest radiograph dataset with uncertainty labels and expert comparison. In *The Thirty-Third AAAI Conference on Artificial Intelligence, AAAI 2019, The Thirty-First Innovative Applications of Artificial Intelligence Conference, IAAI 2019, The Ninth AAAI Symposium on Educational Advances in Artificial Intelligence, EAAI 2019, Honolulu, Hawaii, USA, January 27 - February 1, 2019*, pp. 590–597. AAAI Press, 2019b. doi: 10.1609/AAAI.V33I01.3301590. URL https://doi.org/10.1609/aaai.v33i01.3301590.

Jiang, Y. and Shen, Y. M^{4}oe: A foundation model for medical multimodal image segmentation with mixture of experts. In Linguraru, M. G., Dou, Q., Feragen, A., Giannarou, S., Glocker, B., Lekadir, K., and Schnabel, J. A. (eds.), *Medical Image Computing and Computer Assisted Intervention - MICCAI 2024 - 27th International Conference, Marrakesh, Morocco, October 6-10, 2024, Proceedings, Part XII*, volume 15012 of *Lecture Notes in Computer Science*, pp. 621–631. Springer, 2024. doi: 10.1007/978-3-031-72390-2_58. URL https://doi.org/10.1007/978-3-031-72390-2_58.

Jing, J., Ge, W., Hong, S., Fernandes, M. B., Lin, Z., Yang, C., An, S., Struck, A. F., Herlopian, A., Karakis, I., et al. Development of expert-level classification of seizures and rhythmic and periodic patterns during eeg interpretation. *Neurology*, 100(17): e1750–e1762, 2023a.

Jing, J., Ge, W., Hong, S., Fernandes, M. B., Lin, Z., Yang, C., An, S., Struck, A. F., Herlopian, A., Karakis, I., et al. Development of expert-level classification of seizures and rhythmic and periodic patterns during eeg interpretation. *Neurology*, 100(17): e1750–e1762, 2023b.

Johnson, A. E., Pollard, T. J., Shen, L., Lehman, L.-w. H., Feng, M., Ghassemi, M., Moody, B., Szolovits, P., Anthony Celi, L., and Mark, R. G. Mimic-iii, a freely accessible critical care database. *Scientific data*, 3(1):1–9, 2016.

Johnson, A. E., Bulgarelli, L., Shen, L., Gayles, A., Shammout, A., Horng, S., Pollard, T. J., Hao, S., Moody, B., Gow, B., et al. Mimic-iv, a freely accessible electronic health record dataset. *Scientific data*, 10(1):1, 2023.

Johnson, A. E. W., Pollard, T. J., Berkowitz, S. J., Greenbaum, N. R., Lungren, M. P., Deng, C., Mark, R. G., and Horng, S. MIMIC-CXR: A large publicly available database of labeled chest radiographs. *CoRR*, abs/1901.07042, 2019. URL http://arxiv.org/abs/1901.07042.

Kim, S. Learning general representation of 12-lead electrocar-

diogram with a joint-embedding predictive architecture. *arXiv preprint arXiv:2410.08559*, 2024.

Li, C., Wong, C., Zhang, S., Usuyama, N., Liu, H., Yang, J., Naumann, T., Poon, H., and Gao, J. Llava-med: Training a large language-and-vision assistant for biomedicine in one day. In Oh, A., Naumann, T., Globerson, A., Saenko, K., Hardt, M., and Levine, S. (eds.), *Advances in Neural Information Processing Systems 36: Annual Conference on Neural Information Processing Systems 2023, NeurIPS 2023, New Orleans, LA, USA, December 10 - 16, 2023*, 2023.

Li, H., Ding, M., Zhang, R., and Xiu, C. Motor imagery eeg classification algorithm based on cnn-lstm feature fusion network. *Biomedical signal processing and control*, 72:103342, 2022.

Liang, P. P., Goindani, A., Chafekar, T., Mathur, L., Yu, H., Salakhutdinov, R., and Morency, L.-P. Hemm: Holistic evaluation of multimodal foundation models. In *The Thirty-eight Conference on Neural Information Processing Systems Datasets and Benchmarks Track*, 2024a.

Liang, P. P., Zadeh, A., and Morency, L.-P. Foundations & trends in multimodal machine learning: Principles, challenges, and open questions. *ACM Computing Surveys*, 56(10):1–42, 2024b.

Lin, W., Zhao, Z., Zhang, X., Wu, C., Zhang, Y., Wang, Y., and Xie, W. Pmc-clip: Contrastive language-image pre-training using biomedical documents. *arXiv preprint arXiv:2303.07240*, 2023.

Liu, F., Liu, C., Zhao, L., Zhang, X., Wu, X., Xu, X., Liu, Y., Ma, C., Wei, S., He, Z., et al. An open access database for evaluating the algorithms of electrocardiogram rhythm and morphology abnormality detection. *Journal of Medical Imaging and Health Informatics*, 8(7):1368–1373, 2018.

Liu, Z., Lin, Y., Cao, Y., Hu, H., Wei, Y., Zhang, Z., Lin, S., and Guo, B. Swin transformer: Hierarchical vision transformer using shifted windows. In *2021 IEEE/CVF International Conference on Computer Vision, ICCV 2021, Montreal, QC, Canada, October 10-17, 2021*, pp. 9992–10002. IEEE, 2021. doi: 10.1109/ICCV48922.2021.00986. URL https://doi.org/10.1109/ICCV48922.2021.00986.

Liu, Z., Mao, H., Wu, C., Feichtenhofer, C., Darrell, T., and Xie, S. A convnet for the 2020s. In *IEEE/CVF Conference on Computer Vision and Pattern Recognition, CVPR 2022, New Orleans, LA, USA, June 18-24, 2022*, pp. 11966–11976. IEEE, 2022. doi: 10.1109/CVPR52688.2022.01167. URL https://doi.org/10.1109/CVPR52688.2022.01167.

Lopez, S., Suarez, G., Jungreis, D., Obeid, I., and Picone, J. Automated identification of abnormal adult eegs. In *2015 IEEE signal processing in medicine and biology symposium (SPMB)*, pp. 1–5. IEEE, 2015.

Lopez, S., Gross, A., Yang, S., Golmohammadi, M., Obeid, I., and Picone, J. An analysis of two common reference points for eegs. In *2016 IEEE signal processing in medicine and biology symposium (SPMB)*, pp. 1–5. IEEE, 2016.

Manzari, O. N., Ahmadabadi, H., Kashiani, H., Shokouhi, S. B., and Ayatollahi, A. Medvit: a robust vision transformer for generalized medical image classification. *Computers in Biology and Medicine*, 157:106791, 2023.

Moor, M., Huang, Q., Wu, S., Yasunaga, M., Dalmia, Y., Leskovec, J., Zakka, C., Reis, E. P., and Rajpurkar, P. Med-flamingo: a multimodal medical few-shot learner. In Hegselmann, S., Parziale, A., Shanmugam, D., Tang, S., Asiedu, M. N., Chang, S., Hartvigsen, T., and Singh, H. (eds.), *Machine Learning for Health, ML4H@NeurIPS 2023, 10 December 2023, New Orleans, Louisiana, USA*, volume 225 of *Proceedings of Machine Learning Research*, pp. 353–367. PMLR, 2023. URL https://proceedings.mlr.press/v225/moor23a.html.

Moses, D. A. Deep learning applied to automatic disease detection using chest x-rays. *Journal of Medical Imaging and Radiation Oncology*, 65(5):498–517, 2021.

Nasir, N., Kansal, A., Barneih, F., Al-Shaltone, O., Bonny, T., Al-Shabi, M., and Al Shammaa, A. Multi-modal image classification of covid-19 cases using computed tomography and x-rays scans. *Intelligent Systems with Applications*, 17:200160, 2023.

Nguyen, H. Q., Pham, H. H., Le, T. L., Dao, M., and Lam, K. Vindr-cxr: An open dataset of chest x-rays with radiologist annotations. *PhysioNet*, 2021. doi: 10.13026/3akn-b287. URL https://doi.org/10.13026/3akn-b287.

Ouyang, D., He, B., Ghorbani, A., Yuan, N., Ebinger, J., Langlotz, C. P., Heidenreich, P. A., Harrington, R. A., Liang, D. H., Ashley, E. A., et al. Video-based ai for beat-to-beat assessment of cardiac function. *Nature*, 580(7802):252–256, 2020.

Pacheco, A. G., Lima, G. R., Salomão, A. S., Krohling, B., Biral, I. P., de Angelo, G. G., Alves Jr, F. C., Esgario, J. G., Simora, A. C., Castro, P. B., Rodrigues, F. B., Frasson, P. H., Krohling, R. A., Knidel, H., Santos, M. C., do Espírito Santo, R. B., Macedo, T. L., Canuto, T. R., and de Barros, L. F. Pad-ufes-20: A skin lesion dataset composed of patient data and clinical images collected from smartphones. *Data in Brief*, 32:106221, 2020. doi: 10.1016/j.dib.2020.106221. URL https://doi.org/10.1016/j.dib.2020.106221.

Papatheodorou, I., Fonseca, N. A., Keays, M., Tang, Y. A., Barrera, E., Bazant, W., Burke, M., Füllgrabe, A., Fuentes, A. M.-P., George, N., et al. Expression atlas: gene and protein expression across multiple studies and organisms. *Nucleic acids research*, 46(D1):D246–D251, 2018.

Pedrosa, J., Guilherme, C., Márcio, P., André, J., Eduardo, I., and António, A. Lndb dataset (version 4). In *17th International Conference on Image Analysis and Recognition (ICIAR 2020)*. Zenodo, 2023. doi: 10.5281/zenodo.8348419. URL https://doi.org/10.5281/zenodo.8348419.

Peh, W. Y., Yao, Y., and Dauwels, J. Transformer convolutional neural networks for automated artifact detection in scalp eeg. In *2022 44th Annual International Conference of the IEEE Engineering in Medicine & Biology Society (EMBC)*, pp. 3599–3602. IEEE, 2022.

Pérez-García, F., Sharma, H., Bond-Taylor, S., Bouzid, K., Salvatelli, V., Ilse, M., Bannur, S., Castro, D. C., Schwaighofer, A., Lungren, M. P., et al. Exploring scalable medical image encoders beyond text supervision. *Nature Machine Intelligence*, pp. 1–12, 2025.

Pham, H. H., Nguyen, T. H., and Nguyen, H. Q. Vindr-mammo: A large-scale benchmark dataset for computer-aided detection and diagnosis in full-field digital mammography. *PhysioNet*, 2022. URL https://doi.org/10.13026/br2v-7517.

Philiastides, M. G., Tu, T., and Sajda, P. Inferring macroscale brain

dynamics via fusion of simultaneous eeg-fmri. *Annual Review of Neuroscience*, 44(1):315–334, 2021.

R., S.-L., F., G., A., H., and D., R. Curated breast imaging subset of digital database for screening mammography (cbis-ddsm) [data set], 2016.

Radford, A., Kim, J. W., Hallacy, C., Ramesh, A., Goh, G., Agarwal, S., Sastry, G., Askell, A., Mishkin, P., Clark, J., et al. Learning transferable visual models from natural language supervision. In *International conference on machine learning*, pp. 8748–8763. PMLR, 2021.

Rajendran, S., Pan, W., Sabuncu, M. R., Chen, Y., Zhou, J., and Wang, F. Patchwork learning: A paradigm towards integrative analysis across diverse biomedical data sources. *arXiv preprint arXiv:2305.06217*, 2023.

Rajkomar, A., Dean, J., and Kohane, I. Machine learning in medicine. *New England Journal of Medicine*, 380(14):1347–1358, 2019.

Rajpurkar, P., Chen, E., Banerjee, O., and Topol, E. J. Ai in health and medicine. *Nature medicine*, 28(1):31–38, 2022.

Rotemberg, V., Kurtansky, N., Betz-Stablein, B., and et al. A patient-centric dataset of images and metadata for identifying melanomas using clinical context. *Scientific Data*, 8(1):34, 2021. doi: 10.1038/s41597-021-00815-z. URL https://doi.org/10.1038/s41597-021-00815-z.

Schneider, L., Laiouar-Pedari, S., Kuntz, S., Krieghoff-Henning, E., Hekler, A., Kather, J. N., Gaiser, T., Froehling, S., and Brinker, T. J. Integration of deep learning-based image analysis and genomic data in cancer pathology: A systematic review. *European journal of cancer*, 160:80–91, 2022.

Shaik, T., Tao, X., Li, L., Xie, H., and Velásquez, J. D. A survey of multimodal information fusion for smart healthcare: Mapping the journey from data to wisdom. *Information Fusion*, 102: 102040, 2024.

Sharma, S., Gupta, S., Gupta, D., Juneja, S., Gupta, P., Dhiman, G., and Kautish, S. [retracted] deep learning model for the automatic classification of white blood cells. *Computational Intelligence and Neuroscience*, 2022(1):7384131, 2022.

Sone, K., Toyohara, Y., Taguchi, A., Miyamoto, Y., Tanikawa, M., Uchino-Mori, M., Iriyama, T., Tsuruga, T., and Osuga, Y. Application of artificial intelligence in gynecologic malignancies: A review. *Journal of Obstetrics and Gynaecology Research*, 47 (8):2577–2585, 2021.

Song, Y., Jia, X., Yang, L., and Xie, L. Transformer-based spatial-temporal feature learning for eeg decoding. *arXiv preprint arXiv:2106.11170*, 2021.

Song, Y., Zheng, Q., Liu, B., and Gao, X. Eeg conformer: Convolutional transformer for eeg decoding and visualization. *IEEE Transactions on Neural Systems and Rehabilitation Engineering*, 31:710–719, 2022.

Stark, C., Breitkreutz, B.-J., Reguly, T., Boucher, L., Breitkreutz, A., and Tyers, M. Biogrid: a general repository for interaction datasets. *Nucleic acids research*, 34(suppl_1):D535–D539, 2006.

Takahashi, H., Tampo, H., Arai, Y., Inoue, Y., and Kawashima, H. Applying artificial intelligence to disease staging: Deep

learning for improved staging of diabetic retinopathy. *PloS one*, 12(6):e0179790, 2017.

Thakoor, K. A., Li, X., Tsamis, E., Sajda, P., and Hood, D. C. Enhancing the accuracy of glaucoma detection from oct probability maps using convolutional neural networks. In *2019 41st annual international conference of the IEEE engineering in medicine and biology society (EMBC)*, pp. 2036–2040. IEEE, 2019.

Tschandl, P., Rosendahl, C., and Kittler, H. The HAM10000 dataset: A large collection of multi-source dermatoscopic images of common pigmented skin lesions. *CoRR*, abs/1803.10417, 2018. URL http://arxiv.org/abs/1803.10417.

Tsiknakis, N., Theodoropoulos, D., Manikis, G., Ktistakis, E., Boutsora, O., Berto, A., Scarpa, F., Scarpa, A., Fotiadis, D. I., and Marias, K. Deep learning for diabetic retinopathy detection and classification based on fundus images: A review. *Computers in biology and medicine*, 135:104599, 2021.

Twinanda, A. P., Shehata, S., Mutter, D., Marescaux, J., De Mathelin, M., and Padoy, N. Endonet: a deep architecture for recognition tasks on laparoscopic videos. *IEEE transactions on medical imaging*, 36(1):86–97, 2016.

Vyas, N., Morwani, D., Zhao, R., Shapira, I., Brandfonbrener, D., Janson, L., and Kakade, S. Soap: Improving and stabilizing shampoo using adam. *arXiv preprint arXiv:2409.11321*, 2024.

Wagner, P., Strodthoff, N., Bousseljot, R.-D., Kreiseler, D., Lunze, F. I., Samek, W., and Schaeffter, T. Ptb-xl, a large publicly available electrocardiography dataset. *Scientific data*, 7(1):1–15, 2020.

Wantlin, K., Wu, C., Huang, S.-C., Banerjee, O., Dadabhoy, F., Mehta, V. V., Han, R. W., Cao, F., Narayan, R. R., Colak, E., et al. Benchmd: A benchmark for unified learning on medical images and sensors. *arXiv preprint arXiv:2304.08486*, 2023.

Wie, N. Covid-blues: A large-scale lung ultrasound dataset for covid-19 diagnosis. https://github.com/NinaWie/COVID-BLUES, 2021. Maastricht University Medical Center.

Xia, P., Chen, Z., Tian, J., Gong, Y., Hou, R., Xu, Y., Wu, Z., Fan, Z., Zhou, Y., Zhu, K., Zheng, W., Wang, Z., Wang, X., Zhang, X., Bansal, C., Niethammer, M., Huang, J., Zhu, H., Li, Y., Sun, J., Ge, Z., Li, G., Zou, J., and Yao, H. CARES: A comprehensive benchmark of trustworthiness in medical vision language models. *CoRR*, abs/2406.06007, 2024. doi: 10.48550/ARXIV.2406.06007. URL https://doi.org/10.48550/arXiv.2406.06007.

Yan, X., Wang, W., Xiao, M., Li, Y., and Gao, M. Survival prediction across diverse cancer types using neural networks. In *Proceedings of the 2024 7th International Conference on Machine Vision and Applications*, pp. 134–138, 2024.

Yang, C., Xiao, D., Westover, M. B., and Sun, J. Self-supervised eeg representation learning for automatic sleep staging. *arXiv preprint arXiv:2110.15278*, 2021.

Yang, C., Westover, M., and Sun, J. Biot: Biosignal transformer for cross-data learning in the wild. *Advances in Neural Information Processing Systems*, 36, 2024.

Zhang, X., Wu, C., Zhao, Z., Lin, W., Zhang, Y., Wang, Y., and Xie, W. Pmc-vqa: Visual instruction tuning for medical visual

question answering. *arXiv preprint:2305.10415*, 2023. URL https://doi.org/10.48550/arXiv.2305.10415.

Zheng, J., Chu, H., Struppa, D., Zhang, J., Yacoub, S. M., El-Askary, H., Chang, A., Ehwerhemuepha, L., Abudayyeh, I., Barrett, A., et al. Optimal multi-stage arrhythmia classification approach. *Scientific reports*, 10(1):2898, 2020.

A. Individual Dataset Details

Table 6. **Breakdown of CLIMB dataset by Modalities**

Dataset	# Samples	Clinical Domain	Modality	Task	Fine-grained
PTB-XL	21K	Cardiology	ECG	Diagnostics, Attribute Recognition	/
Chapman-Shaoxing	40K	Cardiology	ECG	Diagnostics	/
Georgia	20K	Cardiology	ECG	Diagnostics	/
CPSC	6K	Sleep Cardiology	ECG	Abnormality Detection	/
IIIC	134.5k	Neurological Disorders	EEG	Diagnostics	/
TUAB	409.5k	Neurological Disorders	EEG	Abnormality Detection	/
TUEV	111.9k	Neurological Disorders	EEG	Diagnostics	/
MIMIC-CXR	356K	Radiology	Chest X-ray	Diagnostics, Classification	No
CheXpert	212K	Radiology	Chest X-ray	Diagnostics, Classification	No
VinDr-CXR	18K	Radiology	Chest X-ray	Diagnostics, Abnormality Detection	Both
COVID-19	2.9K	Radiology	Chest X-ray	Diagnostics	No
CoronaHack	5.9K	Radiology	Chest X-ray	Diagnostics	No
VinDr-Mammo	20K	Radiology, Oncology	Mammography	Diagnostics, Abnormality Detection	Both
CBIS-DDSM	2.8K	Radiology, Oncology	Mammography	Diagnostics, Abnormality Detection, Classification	Both
CMMD	1.8K	Radiology, Oncology	Mammography	Diagnostics, Segmentation, Abnormality Detection	Both
ISIC-2020	33K	Dermatology, Oncology	Dermoscopy	Diagnostics, Classification	No
HAM10000	10K	Dermatology, Oncology	Dermoscopy	Diagnostics, Segmentation	Both
PAD-UFES-20	2.3K	Dermatology, Oncology	Dermoscopy	Diagnostics, Classification	No
Messidor-2	1.7K	Ophthalmology	Fundus	Diagnostics	No
APTOS 2019	3.6K	Ophthalmology	Fundus	Diagnostics	No
Jichi	9.9K	Ophthalmology	Fundus	Diagnostics, Prognostics, Severity Grading	No
LNDb	5.6K	Radiology, Oncology	CT	Diagnostics, Abnormality Detection	Yes
INSPECT	23K	Radiology	CT	Diagnostics, Prognostics	No
KiTS23	478	Radiology, Oncology	CT	Segmentation	Yes
Hemorrhage	2.5K	Radiology	CT	Diagnostics, Segmentation	Both
RSPECT	1.79M	Radiology	CT	Diagnostics, Classification	Yes
EchoNet-Dynamic	10K	Radiology	Ultrasound	Segmentation	Yes
BUSI	780	Radiology, Oncology	Ultrasound	Diagnostics, Segmentation	Both
COVID-BLUES	362	Radiology	Ultrasound	Diagnostics	No
COVID-US	242	Radiology	Ultrasound	Diagnostics, Severity Grading	No
Brain Tumor	3.2K	Radiology, Oncology	MRI	Diagnostics	No
Brain MRI	253	Radiology, Oncology	MRI	Diagnostics	No
ABCD	9.5K	Radiology	BrainNet	Classification	Yes
ABIDE	1009	Radiology	BrainNet	Classification	Yes
PPMI	718	Radiology	BrainNet	Classification	Yes
PROTEINS	1113	Molecular Biology	Molecule	Classification	No
PPI	57K	Molecular Biology	Molecule	Classification	No
LC25000	18.7K	Pathology	Tissues	Classification	No
BCSS	5.26K	Pathology	Tissues	Classification	No
Cholec80	14.4K	Surgery	Video	Workflow Analysis, Segmentation	Yes
HuGaDB	364	Physical Medicine, Rehabilitation	IMU	Motion Analysis, Classification	Yes
Expression Atlas	4.5K	Molecular Biology, Genetics	Gene Expression	Expression Analysis, Classification	Yes
Geo	126K	Molecular Biology, Genetics	Gene Expression	Expression Analysis, Classification	Yes
Vital	210K	Multiple	Multimodal	Diagnostics	Both
MIMIC-IV	800K	Cardiology,Radiology	EHR, ECG, X-ray	Diagnostics, Prognostics, Severity Grading	Both

Table 6 shows a breakdown of the data sources in CLIMB. In this section, we provide details for each dataset. We describe the source and structure of the datasets, split used to evaluate the models, QA prompts, access restrictions, and licenses. A list of classes we constructed is included in Table 7. We also include a list of medical institutions and locations where the data was collected, as well as the demographic info available from each dataset in Table 8.

The definitions of each column are as follows:

Clinical Domain and Modality. Clinical Domain involves the clinical specialty and the exact diseases described by the data. Our dataset aims to cover as many clinical domains as possible. The final dataset spans 13 domains, including radiology, cardiology, pathology, dermatology, oncology, ophthalmology, molecular biology, sleep cardiology and neurological disorders. Within radiology, our dataset spans diseases such as breast cancer, kidney cancer, and pneumonia. Modality involves the type of data at play. Our data ranges from time series (1D), vision (2D & 3D), text records and graphs, making it one of the most diverse datasets up to date.

Task describes the applicable tasks for a multi-modal model. CLIMB spans diagnostics (disease labels), attribute recognition (recognition of inherent structures in the data), abnormality detection (localized abnomality labels), segmentation, prognostics (labels related improvement of condition over time), severity grading, and plain classification (non-disease related labels).

Granularity specifies the level of localization in the task involved. For example, tasks such as segmentation and abnormality

detection requiring localized reasoning and reference to a specific object in an image are classified as fine-grained. In contrast, tasks that make a prediction based on the entire image (e.g. diagnostics) are considered coarse-grained.

Here, we first introduce the list of modalities in CLIMB, followed by a detailed description of each individual dataset.

A.1. List of Modalities

ECG (Electrocardiogram)   Electrocardiogram is a cardiac diagnostic tool that records the electrical activity of the heart over time. The datasets in this modality include {PTB-XL, Chapman-Shaoxing, Georgia, CPSC}, primarily focusing on cardiac diagnostics and abnormality detection. The collective classes across these datasets encompass Normal, Conduction Delay (CD), Hypertrophy (HYP), Myocardial Infarction (MI), Sinus Tachycardia/Bradycardia/Conduction (STTC), Atrial Fibrillation/Atrial Flutter (A. Fib/Aflutter), and Other conditions.

EEG (Electroencephalogram)   EEG is a neurological monitoring method that records brain's electrical activity through electrodes placed on the scalp. The datasets in this category include {IIIC, TUAB, TUEV}, used for diagnosing neurological disorders and detecting abnormalities. The classes across these datasets include Seizure (SZ), Lateralized Periodic Discharges (LPD), Generalized Periodic Discharges (GPD), Lateralized Rhythmic Delta Activity (LRDA), Generalized Rhythmic Delta Activity (GRDA), Spike and Slow Wave (SPSW), Generalized Periodic Epileptiform Discharge (GPED), Periodic Lateralized Epileptiform Discharge (PLED), Eye Movement (EYEM), Artifact (ARTF), Background (BCKG), and simple Normal/Abnormal classifications.

Chest X-ray   Chest X-ray is a radiological imaging technique used to examine the chest cavity, including the heart, lungs, and surrounding structures. The datasets in this modality include {MIMIC-CXR, CheXpert, VinDr-CXR, COVID-19, CoronaHack}. The comprehensive set of classes across these datasets includes Atelectasis, Cardiomegaly, Consolidation, Edema, Enlarged Cardiomediastinum, Fracture, Lung Lesion, Lung Opacity, Pleural Effusion, Pneumonia (including Bacterial and Viral), Pneumothorax, Pleural Other, Support Devices, Lung tumor, Tuberculosis, COPD, COVID-19, and No Finding.

Mammography   Mammography is a specialized medical imaging that uses low-dose X-rays to examine breast tissue for early detection of breast cancer. The datasets in this category include {VinDr-Mammo, CBIS-DDSM, CMMD}. The classes are primarily based on the BI-RADS scoring system (ranging from 0-5) and binary classification of Benign versus Malignant lesions.

Dermoscopy   Dermoscopy is a non-invasive skin imaging technique used for examining skin lesions and early detection of skin cancer. The datasets in this modality include {ISIC-2020, HAM10000, PAD-UFES-20}. The classes across these datasets include Melanoma (MEL), Nevus (NV), Basal Cell Carcinoma (BCC), Actinic Keratosis/Intraepithelial Carcinoma (AKIEC), and Other categories, with some datasets using simple Malignant/Benign classification.

Fundus   Fundus photography is a specialized technique for capturing detailed images of the interior surface of the eye, particularly useful in diagnosing retinal conditions. The datasets include {Messidor-2, APTOS 2019, Jichi}. The classes focus on different stages of Diabetic Retinopathy (DR), including None/No DR, Mild DR, Moderate DR, Severe DR, PDR (Proliferative DR), as well as SDR (simple diabetic retinopathy) and PPDR (pre-proliferative diabetic retinopathy).

CT (Computed Tomography)   CT is an advanced imaging technique that produces detailed cross-sectional images of the body. The datasets in this modality include {LNDb, INSPECT, KiTS23, Hemorrhage, RSPECT}. The classes across these datasets cover various conditions including nodule classification ($\geq$3mm, <3mm, non-nodule), Pulmonary Embolism (PE) categories (No PE, Acute PE, Chronic PE, Subsegmental PE), Hemorrhage detection, and tumor classification (Benign, Malignant).

Ultrasound   Ultrasound imaging uses high-frequency sound waves to produce real-time images of the inside of the body. The datasets include {EchoNet-Dynamic, BUSI, COVID-BLUES, COVID-US}. The classes across these datasets include Normal, Malignant, Benign, COVID-19, and Pneumonia, with some datasets focused on segmentation tasks rather than classification.

MRI (Magnetic Resonance Imaging)   MRI uses magnetic fields and radio waves to create detailed images of organs and tissues. The datasets in this category include {Brain Tumor, Brain MRI}. The classes focus on tumor detection and

classification, including No Tumor, Pituitary Tumor, Glioma Tumor, Meningioma Tumor, and simple presence/absence of tumors.

BrainNet   Brain Network represents brain connectivity networks derived from neuroimaging data. The datasets include {ABCD, ABIDE, PPMI}. The classes focus on binary classifications including Normal/Abnormal, ASD/Typical controls, and Control/PD patients.

Molecule   Molecular data represents structural and functional information about biological molecules. The datasets include {PROTEINS, PPI}, with classification focusing on enzyme/non-enzyme categorization for proteins and molecule property prediction.

Tissues   Tissue imaging from pathology involves microscopic examination of biological tissue samples. The datasets include {LC25000, BCSS}. The classes include various types of adenocarcinomas (Colon, Lung), Benign tissue (Colon, Lung), Lung squamous cell carcinomas, and tissue components (Tumor, Stroma, Lymphocytic infiltrate, Necrosis/debris).

Video   Medical video data captures dynamic medical procedures. The dataset in this category is {Cholec80}, which focuses on surgery phase annotations and tool labels rather than traditional classification tasks.

IMU (Inertial Measurement Unit)   IMU data captures motion and orientation information. The dataset {HuGaDB} includes classes for basic physical activities: Sitting, Standing, Sitting down, and Standing up.

Gene Expression   Gene expression data measures the activity levels of genes. The datasets {Expression Atlas, Geo} are not primarily used for classification tasks but rather for expression analysis.

Multimodal   Multimodal datasets combine multiple types of medical data. The datasets include {Vital, MIMIC-IV}, with MIMIC-IV specifically focusing on 48-hour In-Hospital-Mortality prediction (Yes/No) while combining EHR, ECG, and X-ray data.

A.2. List of Datasets

1. **PTB-XL** (Wagner et al., 2020) is a dataset of 12-lead ECGs from 18,869 patients of 10 second length. The raw waveform data was annotated by two cardiologists, who assigned and validated diagnostic classification, form, and rhythm statements to each record. We provide a grouped label of 7 classes: Normal, CD, HYP, MI, STTC, A. Fib/ Aflutter and Other, following conventions from (Wantlin et al., 2023). For out-of-domain transfer learning, we utilize the subclass diagnostic labels from the PTB-XL dataset, which provides a more challenging 24-label classification task.
   Split: For multitask training, we use the BenchMD split, which includes label remapping to 7 diagnostic categories. This split consists of 17,476 records in the training set and 4,361 records in the test set, totaling 21,837 records.
   Access restrictions: The dataset is available to download from https://physionet.org/files/ptb-xl/1.0.3/
   Licenses: ECG records under this dataset are available in Creative Commons Attribution 4.0 International Public License https://creativecommons.org/licenses/by/4.0/legalcode
   Ethical considerations: No personally identifiable information or offensive content is present in the dataset.

2. **Chapman Shaoxing** (Zheng et al., 2020) consists of 12-lead ECGs from 10,646 patients, created under the auspices of Chapman University and Shaoxing People's Hospital. We provide a grouped label of 7 classes: Normal, CD, HYP, MI, STTC, A. Fib/ Aflutter and Other, following conventions from (Wantlin et al., 2023).
   Split: For multitask training, we use the BenchMD split, which includes label remapping to 7 diagnostic categories. The split consists of 38,207 records in the training set and 2,051 records in the test set, totaling 40,258 records.
   Access restrictions: The dataset is available to download from https://www.kaggle.com/datasets/erarayamorenzomuten/chapmanshaoxing-12lead-ecg-database.

   Licenses: ECG records under this dataset are available in Creative Commons Attribution 4.0 International Public License https://creativecommons.org/licenses/by/4.0/
   Ethical considerations: No personally identifiable information or offensive content is present in the dataset.

3. **Georgia** (Alday et al., 2020) is a database from the 2020 Physionet Computing in Cardiology Challenge, curated by Emory University. It consists of 12-lead ECGs from 15,742 patients of 10 second lengths and 500 Hz frequency, representing a unique demographic of the Southeastern United States. We provide a grouped label of 7 classes: Normal,

CD, HYP, MI, STTC, A. Fib/ Aflutter and Other, following conventions from (Wantlin et al., 2023).
Split: For multitask training, we use the BenchMD split, which includes label remapping to 7 diagnostic categories. The split consists of 18,622 records in the training set and 2,067 records in the test set, totaling 20,689 records.
Access restrictions: The dataset is available to download from https://www.kaggle.com/datasets/bjoernjostein/georgia-12lead-ecg-challenge-database. **Licenses**: ECG records under this dataset are available in Creative Commons Public Domain License https://creativecommons.org/publicdomain/zero/1.0/
Ethical considerations: No personally identifiable information or offensive content is present in the dataset.

4. **CPSC** (Liu et al., 2018) is a database from the 2021 China Physiological Signal Challenge. It consists of 12-lead Holter and 3-lead wearable ECG monitoring device recordings of variable lengths, each sampled at 200 Hz. We provide a grouped label of 7 classes: Normal, CD, HYP, MI, STTC, A. Fib/ Aflutter and Other, following conventions from (Wantlin et al., 2023).
   Split: For multitask training, we use the BenchMD split, which includes label remapping to 7 diagnostic categories. The split consists of 4,815 records in the training set and 1,377 records in the test set, totaling 6,192 records.
   Access restrictions: The dataset is available to download from https://physionet.org/files/cpsc2021/1.0.0/.
   Licenses: ECG records under this dataset are available in Creative Commons Attribution 4.0 International Public License https://creativecommons.org/licenses/by/4.0/legalcode
   Ethical considerations: No personally identifiable information, hospital identification, or offensive content is present in the dataset.

5. **IIIC** (Jing et al., 2023b) consists of EEG samples collected from 2,711 patients at Massachusetts General Hospital, annotated by 124 raters. The publicly available version includes 134,450 EEG segments from 1,950 patients, each segment lasting 10 seconds. The test set is non-public. Our evaluation focuses on the 6 diagnostic categories: seizure (SZ), lateralized periodic discharges (LPD), generalized periodic discharges (GPD), lateralized rhythmic delta activity (LRDA), generalized rhythmic delta activity (GRDA), and "Other" if none of those patterns was present.
   Split: Since the test dataset is not publicly available, we divide patient groups into training/validation/test sets by 60%:20%:20%.
   Access restrictions: The dataset is available to download from https://bdsp.io/content/bdsp-sparcnet/1.1/.
   Licenses: This dataset is available in the BDSP Restricted Health Data License 1.0.0. https://bdsp.io/content/bdsp-sparcnet/view-license/1.1/.
   Ethical considerations: No personally identifiable information or offensive content is present in the dataset.

6. **TUAB** (Lopez et al., 2015) is a dataset from the Temple University EEG Corpus. The dataset consists of 276 EEG recording sessions from 253 subjects. Each session is segmented into 10-second samples using event markers. We evaluate the models based on the binary classification labels "Normal" and "Abnormal."
   Split: The training and test separation is provided by the dataset.
   Access restrictions: The dataset is available to download from https://isip.piconepress.com/projects/nedc/html/tuh_eeg/.
   Licenses: Users must apply using the form described on https://isip.piconepress.com/projects/nedc/html/tuh_eeg/.
   Ethical considerations: No personally identifiable information or offensive content is present in the dataset.

7. **TUEV** (Lopez et al., 2016) is a dataset from the Temple University EEG Corpus. The dataset consists of 518 EEG recording sessions from 368 subjects. Each session is segmented into 5-second samples using event markers. We evaluate the models based on the 6 event categories: spike and slow wave (SPSW), generalized periodic epileptiform discharge (GPED), periodic lateralized epileptiform discharge (PLED), eye movement (EYEM), artifact (ARTF), and background (BCKG).
   Split: The training and test separation is provided by the dataset.
   Access restrictions: The dataset is available to download from https://isip.piconepress.com/projects/nedc/html/tuh_eeg/.
   Licenses: Users must apply using the form described on https://isip.piconepress.com/projects/nedc/html/tuh_eeg/.
   Ethical considerations: No personally identifiable information or offensive content is present in the dataset.

8. **MIMIC-CXR** (Johnson et al., 2019) is a dataset of chest X-rays in JPG format. Our evaluation utilizes the 14 disease labels: "Atelectasis", "Cardiomegaly", "Consolidation", "Edema", "Enlarged Cardiomediastinum", "Fracture", "Lung Lesion", "Lung Opacity", "Pleural Effusion", "Pneumonia", "Pneumothorax", "Pleural Other", "Support Devices", and "No Finding".
   Split: We use a training set of 348,516 records, test set of 7,709 records, and total size of 356,225 records.
   Access restrictions: The dataset is available to download from https://physionet.org/content/mimic-cxr-jpg/2.0.0/ with a credentialed account and CITI Data or Specimens Only Research training

Licenses: Radiology images under this dataset are available in PhysioNet Credentialed Health Data License 1.5.0 https://physionet.org/content/vindr-cxr/view-license/1.0.0/

Ethical considerations: No personally identifiable information or offensive content is present in the dataset.

9. **CheXpert** (Irvin et al., 2019b) is a chest radiology dataset collected from Stanford Hospital, covering 65,240 patients and 224,316 radiographs. The original dataset labels each record with a uncertainty level for 14 diagnostic observations including Atelectasis, Cardiomegaly, Consolidation, Edema, Enlarged Cardiomediastinum, Fracture, Lung Lesion, Lung Opacity, Pleural Effusion, Pneumonia, Pneumothorax, Pleural Other, Support Device and No Finding. Our evaluation focuses on predicting the labels that are "positive".
   Split: We use a training set of 212,243 records, a test set 225 records, and a total size of 212,498 records.
   Access restrictions: The dataset is available to download from https://stanfordaimi.azurewebsites.net/datasets/8cbd9ed4-2eb9-4565-affc-111cf4f7ebe2 with registration
   Licenses: Radiology images under this dataset are available under the Stanford University Dataset Research Use Agreement https://stanfordaimi.azurewebsites.net/datasets/8cbd9ed4-2eb9-4565-affc-111cf4f7ebe2
   Ethical considerations: No personally identifiable information or offensive content is present in the dataset.

10. **VinDr-CXR** (Nguyen et al., 2021) consists of adult chest X-rays collected from Hospital 108 and Hanoi Medical University Hospital in Vietnam. The dataset contains local labels for bounding boxes, however we evaluate our models based on the 6 global labels: "Lung tumor", "Pneumonia", "Tuberculosis", "COPD", "Other diseases", and "No finding", all annotated by 17 radiologists with at least 8 years of experience.
    Split: We use a training set of 15,000 records, a test set of 3,000 records, and a total size of 18,000 records.
    Access restrictions: The dataset is available to download from https://physionet.org/content/vindr-cxr/1.0.0/ with a credentialed account and CITI Data or Specimens Only Research training
    Licenses: Radiology images under this dataset are available in PhysioNet Credentialed Health Data License 1.5.0 https://physionet.org/content/vindr-cxr/view-license/1.0.0/
    Ethical considerations: No personally identifiable information or offensive content is present in the dataset.

11. **COVID-19** is a chest X-ray dataset for COVID-19 related diseases. We evaluate the models based on the diagnostic labels: "Normal", "Bacterial Pneumonia", "COVID-19", and "Viral Pneumonia".
    Split: We use a training set of 2,002 records, a test set of 988 records, and a total size of 2,990 records.
    Access restrictions: The dataset is available to download from https://www.kaggle.com/datasets/darshan1504/covid19-detection-xray-dataset.
    Licenses: This dataset is available in the Creative Commons Attribution 4.0 International License https://creativecommons.org/licenses/by/4.0/
    Ethical considerations: No personally identifiable information or offensive content is present in the dataset.

12. **CoronaHack** (Cohen et al., 2020) is a chest X-ray dataset compiled at the University of Montreal. Our evaluation utilizes the diagnosis labels: "Normal", "Bacterial Pneumonia", and "Viral Pneumonia".
    Split: We use a training set of 5,284 records, a test set of 624 records, and a total size of 5,908 records.
    Access restrictions: The dataset is available to download from https://www.kaggle.com/datasets/praveengovi/coronahack-chest-xraydataset.
    Licenses: This dataset is available in the Creative Commons Attribution 4.0 International License https://creativecommons.org/licenses/by/4.0/
    Ethical considerations: No personally identifiable information or offensive content is present in the dataset.

13. **VinDr-Mammo** (Pham et al., 2022) consists of mammography collected from Hospital 108 and Hanoi Medical University Hospital in Vietnam. The dataset contains local labels for bounding boxes, however we evaluate our models based on the 5 global labels for BI-RAD 1-5.
    Split: We use a training set of 16,000 records, a test set of 4,000 records, and a total size of 20,000 records.
    Access restrictions: The dataset is available to download from https://www.physionet.org/content/vindr-mammo/1.0.0/ with a data use agreement
    Licenses: Images under this dataset are available in PhysioNet Restricted Health Data License 1.5.0 https://www.physionet.org/content/vindr-mammo/view-license/1.0.0/
    Ethical considerations: No personally identifiable information or offensive content is present in the dataset.

14. **CBIS-DDSM** (R. et al., 2016) is a curated subset of the Digital Database for Screening Mammography (DDSM). Our evaluation focuses on the BI-RAD labels (0-5).

Split: We use a training set of 2230 records, a test set of 595 records, and a total of 2,825 records.
Access restrictions: The dataset is available to download from https://www.cancerimagingarchive.net/collection/cbis-ddsm/
Licenses: Images under this dataset are available in Creative Commons Attribution 3.0 Unported License https://creativecommons.org/licenses/by/3.0/
Ethical considerations: No personally identifiable information or offensive content is present in the dataset.

15. **CMMD** (Cui et al., 2021) is a breast mammography dataset for 1,775 patients from China. Our evaluation utilizes the diagnostic labels, "Benign" and "Malignant", which are confirmed through biopsy. However, due to issues found in the provided labels, while this dataset is a part of CLIMB, it is not a part of the experiment while pending expert verifications.
    Split: We use a training set of 1,404 records, a test set of 468 records, and a total size of 1,872 records.
    Access restrictions: The dataset is available to download from https://www.cancerimagingarchive.net/collection/cmmd/.
    Licenses: This dataset is available in the Creative Commons Attribution 4.0 International License https://creativecommons.org/licenses/by/4.0/
    Ethical considerations: No personally identifiable information or offensive content is present in the dataset.

16. **ISIC-2020** (Rotemberg et al., 2021) consists of dermoscopy of skin lesions from over 2000 patients, generated by the International Skin Imaging Collaboration (ISIC). We evaluate the models on the binary classification ("Malignant" or "Benign") for each image, where all malignant diagnoses have been confirmed through histopathology, and benign diagnoses have been confirmed using either expert agreement, longitudinal follow-up, or histopathology.
    Split: We use a training set of 26,501 records, a test set of 6,625 records, and a total size of 33,126 records.
    Access restrictions: The dataset is available to download from https://challenge2020.isic-archive.com
    Licenses: Images under this dataset are available in Creative Commons Attribution-Noncommercial 4.0 International License https://creativecommons.org/licenses/by-nc/4.0/
    Ethical considerations: No personally identifiable information or offensive content is present in the dataset.

17. **HAM10000** (Tschandl et al., 2018) is a dataset from the ISIC 2018 classification challenge, comprising dermoscopy images of pigmented lesions from from the ISIC archive. Our evaluation focuses on the 5 diagnostic categories: Melanoma (MEL), Nevus (NV), Basal Cell Carcinoma (BCC), Actinic Keratosis/Intraepithelial Carcinoma (AKIEC), Other (OTHER)
    Split: We use a training set of 8,012 records, a test set of 2,003 records, and a total size of 10,015 records.
    Access restrictions: The dataset is available to download from https://www.kaggle.com/datasets/kmader/skin-cancer-mnist-ham10000
    Licenses: Images under this dataset are available in Creative Commons Attribution-Noncomercial-Sharealike 4.0 International License https://creativecommons.org/licenses/by-nc-sa/4.0/
    Ethical considerations: No personally identifiable information or offensive content is present in the dataset.

18. **PAD-UFES-20** (Pacheco et al., 2020) consists of dermoscopy images of 1641 skin lesions from 1373 patients. We evaluate the models on the 5 skin diagnostics, three of which are skin disease and three of which are skin cancers: Melanoma (MEL), Nevus (NV), Basal Cell Carcinoma (BCC), Actinic Keratosis/Intraepithelial Carcinoma (AKIEC), Other (OTHER). All of the skin cancers are biopsy-proven, and more than half of the skin disease are biopsy-proven as well.
    Split: We use a training set of 1,839 records, a test set of 459 records, and a total size of 2,298 records.
    Access restrictions: The dataset is available to download from https://www.kaggle.com/datasets/mahdavi1202/skin-cancer
    Licenses: Images under this dataset are available in Creative Commons Attribution 4.0 International License https://creativecommons.org/licenses/by/4.0/
    Ethical considerations: No personally identifiable information or offensive content is present in the dataset.

19. **Messidor-2** (Abràmoff et al., 2013) (Decencière et al., 2014) is a dataset of Diabetic Retinopathy (DR) examinations, where each record consists of two macula-centered eye fundus images. The dataset is kindly provided by the Messidor program partners (see https://www.adcis.net/en/third-party/messidor/). We utilize the 5 point ICDR grades: "None", "Mild DR", "Moderate DR", "Severe DR", and "PDR".
    Split: We use a training set of 1,394 records, a test set of 350 records, and a total size of 1,744 records.
    Access restrictions: The dataset is available to download from https://www.kaggle.com/datasets/google-brain/messidor2-dr-grades.

Licenses: Images under this dataset are available in Creative Commons Public Domain License https://creativecommons.org/publicdomain/zero/1.0/
Ethical considerations: No personally identifiable information or offensive content is present in the dataset.

20. **APTOS 2019** (Asia Pacific Tele-Ophthalmology Society, 2019) is a dataset from the 4th Asia Pacific Tele-Ophthalmology Society Symposium, collected from rural India. The dataset consists of fundus images under a variety of imaging conditions. Our evaluation focuses on the 5 diabetic retinopathy ratings: "No DR", "Mild", "Moderate", "Severe", and "Proliferative DR".
    Split: We use a training set of 2,929 records, a test set of 733 records, and a total size of 3,662 records.
    Access restrictions: The dataset is available to download from https://www.kaggle.com/competitions/aptos2019-blindness-detection/data.
    Licenses: Images under this dataset are available under the Kaggle Competition Rules https://www.kaggle.com/competitions/aptos2019-blindness-detection/rules#7-competition-data
    Ethical considerations: No personally identifiable information or offensive content is present in the dataset.

21. **Jichi** (Takahashi et al., 2017) is a posterior pole fundus photography dataset collected at the Jichi Medical University in Japan, covering a total of 2740 patients. We evaluate the models based on the David Grading for each image: SDR (simple diabetic retinopathy), PPDR (pre-proliferative diabetic retinopathy), and PDR (proliferative diabetic retinopathy).
    Split: We use a training set of 7,950 records, a test set of 1,989 records, and a total size of 9,939 records.
    Access restrictions: The dataset is available to download from https://pmc.ncbi.nlm.nih.gov/articles/PMC5480986/#notes1.
    Licenses: Images under this dataset are available under the Creative Commons Attribution 4.0 International License. https://creativecommons.org/licenses/by/4.0/
    Ethical considerations: No personally identifiable information or offensive content is present in the dataset.

22. **LNDb** (Pedrosa et al., 2023) is lung cancer CT scan dataset collected at the Centro Hispitalar e Universitario de Sao Joao in Portugal between 2016 and 2018. Our evaluation focuses on the pulmonary nodule labels created by radiologists, including "nodule ≥3mm", "nodule <3mm", and "non-nodule".
    Split: We use a training set of 4,130 records, a test set of 1,431 records, and a total size of 5,561 records.
    Access restrictions: The dataset is available to download from https://zenodo.org/records/8348419.
    Licenses: Images under this dataset are available under the Creative Commons Attribution 4.0 International License. https://creativecommons.org/licenses/by/4.0/
    Ethical considerations: No personally identifiable information or offensive content is present in the dataset.

23. **INSPECT** (Huang et al., 2023) is multi-modal dataset containing CT images, radiology report impression sections, and structured electronic health records (EHR) from 19,438 patients. We focus on the pulmonary embolism (PE) labels which include "No PE", "Acute Subsegmental-only PE", "Acute PE", "Subsegmental-only PE", and "Chronic PE".
    Split: We use a training set of 17,434 records, a test set of 5,806 records, and a total size of 23,240 records.
    Access restrictions: The dataset is available to download from https://stanfordaimi.azurewebsites.net/datasets/318f3464-c4b6-4006-9856-6f48ba40ad67 with registration.
    Licenses: This dataset is available under the Stanford University Dataset Research Use Agreement https://stanfordaimi.azurewebsites.net/datasets/318f3464-c4b6-4006-9856-6f48ba40ad67
    Ethical considerations: No personally identifiable information or offensive content is present in the dataset.

24. **KiTS23** (Heller et al., 2023) is a dataset from the 2023 Kidney Tumor Segmentation Challenge. The dataset consists of CT videos showing kidney tumors. Although the data contains metrics and labels for segmentation tasks, we evaluate the models based on the "Benign" and "Malignant" key of each patient.
    Split: We use a training set of 361 records, a test set of 117 records, and a total size of 478 records.
    Access restrictions: The dataset is available to download from https://github.com/neheller/kits23.
    Licenses: This dataset is available in the Creative Commons Attribution-NonCommercial-ShareAlike 4.0 International License https://creativecommons.org/licenses/by-nc-sa/4.0/
    Ethical considerations: No personally identifiable information or offensive content is present in the dataset.

25. **Hemorrhage** (Hssayeni et al., 2020) consists of Intracranial hemorrhage CT images for 82 patients at Al Hilla Teaching Hospital, Iraq, each with brain and bone window images and approximately 30 image slices in total. We evaluate the models on the diagnosis labels "No Hemorrhage" and "Has Hemorrhage".
    Split: We use a training set of 1,986 records, a test set of 515 patient records, and a total size of 2,501 records.

Access restrictions: The dataset is available to download from https://www.kaggle.com/datasets/vbookshelf/computed-tomography-ct-imagesc .
Licenses: This dataset is available in the Creative Commons Attribution 4.0 International Public License https://physionet.org/content/ct-ich/view-license/1.0.0/
Ethical considerations: No personally identifiable information or offensive content is present in the dataset.

26. **RSPECT** (Colak et al., 2021) consists of CT scans for patients from five different countries suspected of Pulmonary Embolism (PE), created by the Radiological Society of North America (RSNA) and the Society of Thoracic Radiology (STR). We evaluate the models on the diagnosis labels "No PE", "Chronic PE", and "Acute PE", which are annotated by expert thoracic radiologists.
    Split: We use a training set of 1,342,945 records, a test set of 447,649 records, and a total size of 1,790,594 records.
    Access restrictions: The dataset is available to download from https://www.kaggle.com/c/rsna-str-pulmonary-embolism-detection/data.
    Licenses: This dataset is available in under the Kaggle competition rules https://www.kaggle.com/competitions/rsna-str-pulmonary-embolism-detection/data
    Ethical considerations: No personally identifiable information or offensive content is present in the dataset.

27. **EchoNet-Dynamic** (Ouyang et al., 2020) consists of 10,030 apical-4-chamber echocardiography videos from patients who underwent imaging between 2016 and 2018 as part of routine clinical care at Stanford University Hospital. Each video comes with two pairs of human tracings used to estimate ventricular volume—the first pair representing the left ventricle, and subsequent coordinate pairs representing short axis linear distances starting from the apex of the heart to the mitral apparatus.
    Split: We use a training set of 8,196 records, a test of 2,051 records, and a total size of 10,247 records.
    Access restrictions: The dataset is available to download from https://stanfordaimi.azurewebsites.net/datasets/834e1cd1-92f7-4268-9daa-d359198b310a with registration.
    Licenses: This dataset is available under the Stanford University Dataset Research Use Agreement https://stanfordaimi.azurewebsites.net/datasets/834e1cd1-92f7-4268-9daa-d359198b310a
    Ethical considerations: No personally identifiable information or offensive content is present in the dataset.

28. **BUSI** (Al-Dhabyani et al., 2020) is a breast cancer ultrasound image dataset from 600 female patients between 25 and 75 years old in 2018. We utilize the labels "Normal", "Malignant", and "Benign".
    Split: We use a training set of 583 records, a test set of 197 records, and a total size of 780 records.
    Access restrictions: The dataset is available to download from https://www.kaggle.com/datasets/aryashah2k/breast-ultrasound-images-dataset.
    Licenses: This dataset is available in the Creative Commons Public Domain License https://creativecommons.org/publicdomain/zero/1.0/
    Ethical considerations: No personally identifiable information or offensive content is present in the dataset.

29. **COVID-BLUES** (Wie, 2021) consists of bluepoint-specific lung ultrasound videos for 63 patients at the Maastricht University Medical Center in the Netherlands, each with 6 recordings. Our evaluation focuses on two labels: the diagnostic label ("Has COVID", "No COVID"), and the patient age label.
    Split: We use a training set of 266 records, a test set of 96 records, and a total size of 362 records.
    Access restrictions: The dataset is available to download from https://github.com/NinaWie/COVID-BLUES?tab=readme-ov-file.
    Licenses: This dataset is available in the Creative Commons Attribution-Noncommercial-NoDerivatives 4.0 International License https://creativecommons.org/licenses/by-nc-nd/4.0/
    Ethical considerations: No personally identifiable information or offensive content is present in the dataset.

30. **COVID-US** (Ebadi et al., 2021) consists of 150 COVID-related lung ultrasound videos. We evaluate the models based on the diagnostic labels: "Covid", "Pneumonia", and "Normal".
    Split: We use a training set of 74 records, a test set of 25 records, and a total size of 99 records.
    Access restrictions: The dataset is available to download from https://github.com/nrc-cnrc/COVID-US.
    Licenses: This dataset is available in the GNU Affero General Public License 3.0 https://www.gnu.org/licenses/agpl-3.0.en.html
    Ethical considerations: No personally identifiable information or offensive content is present in the dataset.

31. **Brain Tumor** (Bhuvaji et al., 2020) consists of brain MRI images. Each image is labeled as either "No Tumor",

"Pituitary Tumor", "Glioma Tumor", or "Meningioma Tumor".

Split: We use a training set of 2,870 records, a test set of 394 records, and a total size of 3,264 records.

Access restrictions: The dataset is available to download from https://www.kaggle.com/datasets/sartajbhuvaji/brain-tumor-classification-mri?select=Testing.

Licenses: This dataset is available in the MIT License https://www.mit.edu/ amini/LICENSE.md

Ethical considerations: No personally identifiable information or offensive content is present in the dataset.

32. **Brain MRI** is a brain MRI image dataset where each image is labeled with the presence of tumors, either as "Yes" or "No".

     Split: We use a training set of 202 records, a test set of 51 records, and a total size of 253 records.

     Access restrictions: The dataset is available to download from https://www.kaggle.com/datasets/jjprotube/brain-mri-images-for-brain-tumor-detection.

     Licenses: This dataset does not have a license.

     Ethical considerations: No personally identifiable information or offensive content is present in the dataset.

33. **ABCD** (Cui et al., 2022) is a study supported by the NIH on adolescent brain cognitive development on nearly 12,000 youths of ages 9-10, who were studied for 10 years. The dataset contains MRI images, behavioral and cognitive assessments, mental health, and other environmental factors data, with labels such as mental health diagnosis. In our dataset, we do a mental health diagnosis that classifies the sample into normal and abnormal.

     Split: The dataset has a total of 9563 records. We randomly split the dataset into a train set of 7650 and a test dataset of 1613 records.

     Access restrictions: The dataset is available to download from Link.

     Licenses: The license is available at Link.

     Ethical considerations: No personally identifiable information or offensive content is present in the dataset.

34. **ABIDE** (Cui et al., 2022) is a autism brain MRI diagnosis dataset with 1112 samples, including 539 from individuals with ASD and 573 from typical controls.

     Split: We use a random split to build a training set of 807 records, a test set of 202 records, and a total size of 1009 records.

     Access restrictions: The dataset is available to download from https://fcon_1000.projects.nitrc.org/indi/abide/ with account registration.

     Licenses: The dataset is available in the Creative Commons Attribution-NonCommercial-Share Alike License https://creativecommons.org/licenses/by-nc-sa/3.0/.

     Ethical considerations: No personally identifiable information or offensive content is present in the dataset.

35. **PPMI** (Cui et al., 2022) is a multi-center, longitudinal study dedicated to understanding the progression of Parkinson's disease. This data is derived from a cohort of 1694 subjects, broken down into 309 controls and 1385 PD patients.

     Split: After curation, we use random split to build a training set of 572 records, a test set of 143 records, and a total size of 718 records.

     Access restrictions: The dataset is available to download from Link.

     Licenses: The license is available in the Link.

     Ethical considerations: No personally identifiable information or offensive content is present in the dataset.

36. **PROTEINS** (Borgwardt et al., 2005) consists of 1,113 graphs where the nodes represent amino acids, and two nodes are connected by an edge if they are less than 6 Angstroms apart. We evaluate our models on the binary classification labels of whether a protein is an enzyme or not.

     Split: We use random split to build a training set of 890 records, a test set of 223 records, and a total size of 1,113 records.

     Access restrictions: The dataset is available to download from https://paperswithcode.com/dataset/proteins.

     Licenses: The dataset does not have a license.

     Ethical considerations: No personally identifiable information or offensive content is present in the dataset.

37. **PPI** (Stark et al., 2006) is a protein dataset from BioGRID covering physical and genetic interaction of proteins.

     Split: We use a training set of 45555 records, a test set of 11389 records, and a total size of 56944 records.

     Access restrictions: The dataset is available to download from https://snap.stanford.edu/graphsage/#datasets.

     Licenses: The dataset is available in the MIT License https://biogrid-downloads.nyc3.digitaloceanspaces.com/LICENSE.txt.

Ethical considerations: No personally identifiable information or offensive content is present in the dataset.

38. **LC25000** (Borkowski et al., 2019) is a lung and colon histopathological image dataset containg labels for colon adenocarcinomas, benign colon, lung adenocarcinomas, lung squamous cell carcinomas, and benign lung.
    Split: We use a training set of 15,000 records, a test set of 3,750 records, and a total size of 18,750 records.
    Access restrictions: The dataset is available to download from https://github.com/tampapath/lung_colon_image_set.
    Licenses: The dataset does not have a license.
    Ethical considerations: No personally identifiable information or offensive content is present in the dataset.

39. **BCSS** contains 151 breast cancer slides from 25 participants. We curate 5264 non-overlapping samples, with labels tumor, stroma, lymphocytic infiltrate, and necrosis/debris
    Split: We use a training set of 4211 records, a test set of 1053 records, and a total size of 5264 records.
    Access restrictions: The dataset is available to download from Link.
    Licenses: This dataset is licensed under a CC0 1.0 Universal (CC0 1.0) license.
    Ethical considerations: No personally identifiable information or offensive content is present in the dataset.

40. **Cholec80** (Twinanda et al., 2016) consists of 80 videos of cholecystectomy surgeries performed by 13 surgeons. We evaluate the models based on the surgery phase annotations (at 25 fps) and the surgery tool labels (at 1 fps).
    Split: We use a training set of 5,760 records, a test set of 1,440, and a total size of 7,200 records.
    Access restrictions: The dataset is available to download from http://camma.u-strasbg.fr/datasets/ through a request form.
    Licenses: This dataset is available in the Creative Commons Attribution-Noncomercial-Sharealike 4.0 International License https://creativecommons.org/licenses/by-nc-sa/4.0/legalcode.en
    Ethical considerations: No personally identifiable information or offensive content is present in the dataset.

41. **HuGaDB** (Chereshnev & Kertész-Farkas, 2018) is a dataset for human gait analysis collected from 18 healthy young adults using six wearable inertial sensors and two EMG sensors. It contains labels "sitting", "standing", "sitting down", and "standing up". However, due to the limitation of the number of samples, this gait dataset is not included in the experiments.
    Split: We use a training set of 291 records, a test set of 73 records, and a total size of 364 records.
    Access restrictions: The dataset is available to download from https://github.com/romancheresnev/HuGaDB.
    Licenses: The dataset does not have a license.
    Ethical considerations: No personally identifiable information or offensive content is present in the dataset.

42. **Expression Atlas** (Papatheodorou et al., 2018) consists of RNA gene expression data across species and biological conditions.
    Split: We use a training set of 3605 records, a test set of 901 records, and a total size of 4,506 records.
    Access restrictions: The dataset is available to download from https://www.ebi.ac.uk/gxa/download.
    Licenses: This dataset is available in the Creative Commons Attribution-Noncommercial-NoDerivatives 4.0 International License https://creativecommons.org/licenses/by-nc-nd/4.0/.
    Ethical considerations: No personally identifiable information or offensive content is present in the dataset.

43. **Geo** is a functional genomics dataset supporting MIAME-compliant data submissions.
    Split: We use a training set of 101162 records, a test set of 25290 records, and a total size of 126,452 records.
    Access restrictions: The dataset is available to download from https://www.ncbi.nlm.nih.gov/geo/.
    Licenses: The license is available at Link.
    Ethical considerations: No personally identifiable information or offensive content is present in the dataset.

44. **Vital** (Cui et al., 2024) is a medical image-language dataset based on PMC-15, where instructional data is generated using the gpt-4-vision-preview API.
    Split: We use a training set of 42000 records, a test set of 168000 records, and a total size of 210,000 records.
    Access restrictions: The dataset is available to download from https://huggingface.co/datasets/mao1207/BioMed-VITAL-instructions.
    Licenses: The dataset is available in Apache License 2.0 https://www.apache.org/licenses/LICENSE-2.0.
    Ethical considerations: No personally identifiable information or offensive content is present in the dataset.

45. **MIMIC-IV** (Johnson et al., 2023) (Johnson et al., 2016) (Goldberger et al., 2000) is a multimodal medical dataset on patients admitted to the emergency department or intesnive care unit at the Beth Israel Deaconess Medical Center in Boston, MA. We train and evaluate our models using the EHR, vital sign, and chest-xray modalities.

Split: CLIMB provide a training set of 640,000 records, a test set of 160,000 records, and a total size of 800,000 records. In the fusion experiment, however, we focus on the multimodal subset of MIMIC-IV, which contains 166,215 training samples, 41,554 test samples, and 207769 total samples.

Access restrictions: The dataset is available to download from https://physionet.org/content/mimiciv/3.1/ with credentialed account and CITI training.

Licenses: The dataset is available in PhysioNet Credentialed Health Data License 1.5.0 https://physionet.org/content/mimiciv/view-license/3.1/.

Ethical considerations: No personally identifiable information or offensive content is present in the dataset.

Dataset Selection Methodology

Our dataset collection and curation process follows a systematic two-stage approach to ensure both comprehensive coverage and accessibility while maintaining data quality and diversity.

Stage 1: Initial Dataset Identification

We first conducted a comprehensive literature review of publicly available clinical datasets across different modalities. Our inclusion criteria at this stage focused on accessibility:

- Datasets with direct download access through public repositories

- Datasets requiring application but with clear, less restrictive licensing terms

- Datasets with well-documented data collection protocols and annotation procedures

We explicitly excluded datasets that:

- Require institutional review board (IRB) approval

- Have restrictive licensing terms limiting research use

Stage 2: Selection and Prioritization

In the second stage, we applied a two-tier selection process:

- **Tier 1:** We first included widely-cited benchmark datasets that serve as standard evaluation metrics in their respective domains. These datasets were identified based on citation count and frequency of use in published literature. Examples include CheXpert and MIMIC-IV.

- **Tier 2:** We then systematically identified and included datasets that addressed our three key criteria:

  - Novel tasks: Datasets covering emerging clinical challenges (e.g., COVID-19 diagnosis)
  - Understudied modalities: Datasets from underrepresented data types (e.g., EEG, endoscopic videos)
  - Underrepresented regions: Datasets from developing regions with limited representation

Selection Criteria

Here, we elaborate on our methodology for identifying understudied modalities and underrepresented regions during the stage 2 selection.

Understudied Modalities. We evaluated modalities from two complementary perspectives:

1. **Research Attention:** We quantified research activity by aggregating Google Scholar search results using standardized queries (e.g., '[Modality] classification', '[Modality] machine learning'). Our analysis revealed significant disparities in research attention across modalities:

   - High attention (>1M articles): Pathology (1.38M), X-ray (1.08M), CT Scan (2.83M), Endoscopic (1.74M)
   - Medium attention (300K-1M): MRI (931K), Dermoscopy (530K), Ultrasound (636K), Fundus (848K), EEG (450K)
   - Low attention (<500K): Mammography (56.1K), ECG (265K)

2. **Data Availability:** We analyzed the total number of publicly available samples per modality:

   - High availability (>500K): X-ray (595,264), CT Scan (1,810,256), EEG (655,786)

- Medium availability (50K-500K): ECG (84,172), Genomic (130,958)
- Low availability (5K-50K): Mammography (24,697), Dermoscopy (45,439), Fundus (18,067), Endoscopic (14,400), Pathology (24,014), MRI (14,807)
- Very low availability (<5k): Ultrasound (1,633)

Based on this analysis, we identified several critically understudied modalities. Mammography and ECG emerged as understudied based on research attention, while ultrasound was identified as understudied due to extremely limited public data availability (1,633 samples). These findings guided our focused efforts to collect additional datasets in these modalities.

Underrepresented Regions. We also employed a two-step approach to identify geographic gaps in dataset coverage:

1. **Geographic Distribution:** We created a global heatmap of dataset origins, revealing significant underrepresentation in:

   - Africa
   - South America
   - Parts of South and Southeast Asia

2. **Economic Development:** We mapped datasets to their countries of origin, specifically identifying datasets from developing nations. This analysis highlighted the importance of including datasets from:

   - Asia: India, Vietnam
   - Middle East: Iraq
   - South America: Brazil

This analysis informed our targeted efforts to include datasets from these underrepresented regions, aiming to improve the geographic and demographic diversity of our benchmark. The complete list of included datasets and their geographic distribution is provided in Table X.

Data Preprocessing and Standardization

To preserve data fidelity while ensuring usability, we implemented minimal preprocessing steps:

- **Time Series Data (ECG/EEG):**

  - Standardized sampling rates across datasets
  - Normalized amplitude ranges
  - Preserved original waveform characteristics

- **Imaging Data:**

  - Maintained original image resolution and quality
  - Created standardized JSON metadata files linking:
    * Clinical labels
    * Demographic information
    * Multi-view relationships
    * Additional annotations (where available)

No preprocessing was done on graph data, as they are already processed and ready to use.

All additional metadata and multi-view images are preserved and made available, though our benchmark experiments utilize only the primary labels to ensure fair comparison across models. The complete preprocessing scripts and documentation are available in our code repository.

B. CLIMB-QA Construction

To enable standardized evaluation of large vision-language models (VLMs), we construct CLIMB-QA, a question-answering version of our dataset. For each sample $x_i \in D_k$ with label set $y_i \subseteq V_k$, we generate a question-answer pair (q_i, a_i) where:

- q_i is constructed as a natural language question incorporating:

- – Task description (e.g., "grade the diabetic retinopathy")
- – Input modality context (e.g., "in the retinal image")
- – Available choices from the label vocabulary V_k

- a_i is the ground truth answer derived from y_i, formatted as either:

  - – Single-label: $a_i \in V_k$ for mutually exclusive classes
  - – Multi-label: $a_i \subseteq V_k$ for compatible conditions

Formally, we define a mapping function $\psi : (x_i, y_i, V_k) \rightarrow (q_i, a_i)$ that generates question-answer pairs while preserving the original classification task structure. For example, in the APTOS dataset for diabetic retinopathy grading:

$q_i =$ "Above is a retinal image of a patient. Grade the diabetic retinopathy on the Davis Scale, choosing from: No DR, Mild DR, Moderate DR, Severe DR, Proliferative DR."

$a_i =$ "Moderate DR"

For multi-label classification tasks, we evaluate predictions using order-agnostic matching: given a predicted answer set $\hat{a}_i$ and ground truth a_i, we consider the prediction correct if $\hat{a}_i = a_i$ regardless of the order in which the labels are listed. This ensures fair evaluation when multiple conditions are present and can be enumerated in any order.

C. Detailed Experimental Setup

C.1. Problem Definition

RQ1/RQ2: We use the definition of the dataset as well as the vocabularies as defined in Sec. 3.2. For each input sample $x_i \in \mathcal{X}$, which can be an image, video, or multi-channel time series, we extract n sequential elements. The input processing varies by modality:

1. Images: $\phi_{img} : \mathbb{R}^{H \times W \times C} \to \mathbb{R}^{n \times \sigma \times \sigma \times C}$

2. Videos: $\phi_{vid} : \mathbb{R}^{T \times H \times W \times C} \to \mathbb{R}^{n \times \sigma \times \sigma \times C}$

3. Time Series: $\phi_{ts} : \mathbb{R}^{T \times C} \to \mathbb{R}^{n \times C}$

where σ denotes the model-specific input size, and H, W, C, T represent spatial dimensions, channels, and temporal length, respectively. The objective is to learn a function $f : \mathcal{X} \to \{0,1\}^{|\mathcal{V}|}$ that maps each input to a binary vector over $\mathcal{V}$.

RQ3: Given multimodal inputs $\mathcal{M} = m_{vis}, m_{lang}, m_{ts}$, where each modality-specific input $x_i^m \in \mathcal{X}^m$ corresponds to visual, language, and time series data respectively, the model aims to learn two prediction functions:

1. In-hospital Mortality in 48 hours (IHM 48): Binary prediction $f_{ihm} : \prod_{m \in \mathcal{M}} \mathcal{X}^m \to \{0,1\}$ predicting 48-hour mortality

2. Length of Stay: Regression function $f_{los} : \prod_{m \in \mathcal{M}} \mathcal{X}^m \to \mathbb{R}^+$ estimating the expected duration of hospitalization.

C.2. Experimental Procedures

To answer the above research questions, we design our experiments as follows:

C.2.1. RQ1: UNIVERSAL ENCODERS PERFORMANCE UNDER MULTITASK LEARNING.

We investigate how can we build a universal encoder for each input type across all clinical tasks. Specifically, we train vision, graph and time series encoders on the complete $\mathcal{D}$ to assess general diagnostic capabilities. For each sample $x_i \in D_k$, we evaluate performance using a dataset-specific vocabulary mask $\mathbb{1}_{V_k} \in \{0,1\}^{|\mathcal{V}|}$, where only predictions corresponding to labels in V_k are considered in the evaluation metrics. Performance is measured using Area Under the ROC Curve (AUC) and binary classification metrics (specificity and sensitivity) with a decision threshold of 0.5 over the masked label space $\mathcal{V} \odot \mathbb{1}_{V_k}$. In addition, we compare the results pre-trained on our entire datasets against those just pre-trained on each target dataset, exploring the effect of large-scale pre-training on the model's performance.

C.2.2. RQ2: TRANSFER LEARNING UNDER RESOURCE CONSTRAINTS.

Second, we evaluate few-shot generalization on out-of-distribution (OOD) datasets $\mathcal{D}_{ood} \not\subset \mathcal{D}_{train}$, where $\mathcal{D}_{ood}$ contains novel label sets V_{ood} such that $V_{ood} \cap \mathcal{V} = \emptyset$ within the same modality. This setup simulates the practical scenario where models must adapt to novel diagnostic tasks with limited labeled examples while leveraging pre-trained representations from related but distinct tasks. A detailed description of the dataset composition, as well as the experimental procedure, are included in App. C.7.1.

C.2.3. RQ3: SINGLE MODALITY TO MULTIMODALITY TRANSFER VIA ROBUST FUSION STRATEGY.

Finally, we investigate optimal fusion mechanisms for integrating heterogeneous modalities as defined in App. C.1. We evaluate three fusion architectures $g_\theta : \prod_{m \in \mathcal{M}} \mathbb{R}^{d_m} \to \mathbb{R}^d$:

1. late fusion g_{late} that averages predictions from modality-specific classifiers: $g_{late}(h_m) = \frac{1}{|\mathcal{M}|} \sum_{m \in \mathcal{M}} \text{MLP}_m(h_m)$,

2. simple concatenation followed by two-layer MLP $g_{mlp}(h_m) = \text{MLP}(\text{Concat}([h_{vis}, h_{lang}, h_{ts}]))$, and

3. cross-modal attention g_{attn} that uses text features to form queries and concatenated vision/time-series features for keys and values, computing $g_{attn}(h_m) = \text{FFN}(\text{softmax}(\frac{QK^T}{\sqrt{d}})V)$ where $Q = h_{lang}W_Q$, $K = \text{Concat}([h_{vis}, h_{ts}])W_K$, $V = \text{Concat}([h_{vis}, h_{ts}])W_V$

For controlled comparison, we fix the backbone encoders across all fusion strategies: ConvNextv2 (Liu et al., 2022) for visual inputs, ClinicalBERT (Huang et al., 2019) for text, and ECG-JEPA (Kim, 2024) for time series data.

C.3. Evaluation Metrics

For binary classification tasks $f : \mathcal{X} \to \{0,1\}$, we employ three complementary metrics to assess model performance:

1. Area Under the ROC Curve (AUC): Given predicted probabilities $\hat{y}_i \in [0, 1]$ and true labels $y_i \in \{0, 1\}$, AUC measures the model's ability to discriminate between classes across all possible decision thresholds:

$$\text{AUC} = \int_0^1 \text{TPR}(t)\text{FPR}'(t)dt$$

    where TPR(t) and FPR(t) are the true positive and false positive rates at threshold t.

2. Sensitivity (also known as recall): Measures the model's ability to correctly identify positive cases:

$$\text{Sensitivity} = \frac{\text{TP}}{\text{TP} + \text{FN}}$$

    where TP and FN denote true positives and false negatives respectively.

3. Specificity: Quantifies the model's ability to correctly identify negative cases:

$$\text{Specificity} = \frac{\text{TN}}{\text{TN} + \text{FP}}$$

    where TN and FP denote true negatives and false positives respectively.

The choice of these three metrics is particularly motivated by clinical considerations. In medical diagnosis, there is often an inherent trade-off between sensitivity and specificity, where improving one typically comes at the cost of the other. Sensitivity is crucial in cases where missing a positive diagnosis (false negative) could have severe consequences for patient outcomes, such as failing to detect a life-threatening condition. Conversely, specificity is vital when false positives could lead to unnecessary interventions, psychological distress, or resource waste.

AUC provides a threshold-independent measure of discriminative ability, making it particularly valuable for comparing models across different operating points and clinical contexts. This is especially relevant in our multi-task setting where different clinical applications may require different sensitivity-specificity trade-offs.

For regression tasks such as length of stay prediction (f_{los}), we use Mean Absolute Error (MAE):

$$\text{MAE} = \frac{1}{n}\sum_{i=1}^{n}|y_i - \hat{y}_i|$$

where y_i and $\hat{y}_i$ represent the true and predicted values respectively. All metrics are computed using the dataset-specific vocabulary masks $\mathbb{1}_{V_k}$ as defined in Sec. C.1.

Below, we describe in detail about the setup and procedures of vision, time series and graph experiments.

C.4. Vision Model Experiments
C.4.1. VISION MODEL DETAILS
MedViT (Manzari et al., 2023) is a Vision Transformer variant specifically designed for medical imaging tasks. It incorporates a hierarchical structure with varying token sizes across different stages and employs medical-specific attention mechanisms optimized for capturing fine-grained anatomical details.

PMC-CLIP (Lin et al., 2023) adapts the CLIP architecture for medical imaging by pretraining on PubMed Central articles and their associated figures. It maintains the original dual-encoder structure but incorporates medical domain knowledge through specialized text-image contrastive learning.

RAD-DINO (Pérez-García et al., 2025) extends the DINO self-supervised learning framework to radiology images. It employs specialized augmentation strategies and anatomical consistency constraints during the self-supervised pretraining process to better capture medical imaging characteristics.

SBB2 (Radford et al., 2021) is an enhanced vision backbone that builds upon the clip architecture. It introduces improved spatial mixing operations and hierarchical feature representations while maintaining computational efficiency.

Swin Transformer (Liu et al., 2021) is a hierarchical vision transformer that computes self-attention within shifted windows. It introduces a hierarchical architecture with varying window sizes across different stages, enabling efficient modeling of both local and global dependencies.

EVA-2 (Fang et al., 2024) is a large-scale vision foundation model that extends the original EVA architecture. It utilizes masked image modeling and contrastive learning objectives, incorporating improvements in model scaling and training strategies.

InternViT (Chen et al., 2023) is a vision transformer model that introduces internalized attention mechanisms. It optimizes the traditional transformer architecture for improved efficiency while maintaining performance across diverse visual tasks.

ConvNeXTv2 (Liu et al., 2022) is a pure convolutional architecture that modernizes traditional CNN design principles. It incorporates fully convolutional design, global response normalization, and gradient checkpointing, achieving strong performance across various vision tasks.

C.4.2. VISION HYPERPARAMETERS AND EXPERIMENTAL PROCEDURES

All experiments are ran on a GPU server with 8xH200 141GB GPUs. We used the SOAP optimizer (Vyas et al., 2024) as it offers the best performance. Depending on the model sizes, we use a parameter search to identify the optimal learning rate from 1×10^{-5} to 1×10^{-3} for all experiments. The weight decay was set to 1×10^{-3}. We use a parameter search to find the largest GPU that could fit on a single server. All experiments were conducted using the PyTorch framework. We saved the model with the lowest $CrossEntropy$ loss over 5 epochs for evaluation on the test split. We report the AUROC, Sensitivity, Specificity, F1 Score and accuracy of our experiments in App. D.

C.5. EEG Model Experiments

We investigate the performance of five baseline models and four variants of foundational time series models for EEG classifications. Our EEG experiment is built upon the repository sheared by (Yang et al., 2024), and the pre-trained weights were downloaded from `https://github.com/ycq091044/BIOT`.

C.5.1. EEG DATASETS AND PREPROCESSING

We evaluated the models on IIIC (Jing et al., 2023b), TUAB (Lopez et al., 2015), and TUEV (Lopez et al., 2016). All EEG channels, $S[i]$, in each individual sample were resampled to 200 Hz and normalized using the 95th percentile of the absolute amplitude:

$$\frac{\mathbf{S}^{[i]}}{\text{percentile}([|\mathbf{S}[i,1]|, |\mathbf{S}[i,2]|, \ldots, |\mathbf{S}[i,J]|], 95\%)}$$

For details on dataset access and data splitting, please refer to App. A.

C.5.2. EEG HYPERPARAMETERS AND EXPERIMENTAL PROCEDURES

We used the Adam optimizer (Diederik, 2014) with a learning rate of 1×10^{-3} for all experiments. The weight decay was set to 1×10^{-5}. For most experiments, the batch size was set to 512, while for few-shot experiments, it was set to 4. All experiments were conducted using the PyTorch framework. We saved the model with the lowest $CrossEntropy$ loss over 20 epochs for evaluation on the test split. We report the AUROC, Sensitivity, Specificity, and F1 Score of our experiments in App. D.

C.5.3. EEG MODEL DETAILS

SPaRCNet (Jing et al., 2023b) is a 1D-CNN designed for EEG classification. It employs a hierarchical feature extraction process, beginning with an initial convolutional layer followed by multiple densely connected blocks and transition layers. The model integrates ELU activation functions, batch normalization, and dropout for improved generalization.

CNNTransformer (Peh et al., 2022) is a hybrid deep learning model that combines convolutional neural networks (CNNs) with a Transformer encoder for EEG classification. The model first applies short-time Fourier transform (STFT) to extract spectral representations, which are then processed through a deep residual CNN with four stacked *ResBlocks* for hierarchical feature extraction. The CNN embeddings are segmented and passed through a Transformer encoder with positional encoding, allowing the model to capture long-range temporal dependencies.

ContraWR (Yang et al., 2021) is a EEG classification model that integrates STFT with a 2D-CNN for sleep staging. The model first converts raw EEG signals into spectrograms using STFT, which are then processed through a deep residual CNN

with four stacked *ResBlocks*, each employing batch normalization, dropout, and max pooling for feature extraction.

FFCL (Li et al., 2022) is a hybrid CNN-LSTM model designed for EEG classification, integrating both spectral and temporal feature representations. The model first apply STFT to extract frequency-domain features, which are then processed through a deep residual CNN with four stacked *ResBlocks*. In parallel, the raw EEG signals undergo temporal compression using a downsampling operation before being fed into a bidirectional LSTM for sequential feature extraction. The final representation is obtained by concatenating CNN and LSTM embeddings, which are passed through a fully connected classification layer.

STTransformer (Song et al., 2021) is a spatiotemporal Transformer model for EEG classification that integrates channel-wise attention with Transformer-based sequence modeling. The model first applies a *ChannelAttention* mechanism to capture inter-channel dependencies, followed by a *PatchSTEmbedding* module that encodes local temporal structures. These embeddings are then processed through a deep Transformer encoder, which models long-range dependencies and contextual information. The v2.0 of STTransformer is known as EEG-Conformer (Song et al., 2022).

BIOT (Yang et al., 2024) is a biosignal transformer model designed for cross-data learning in the wild, enabling robust representation learning across diverse biosignal modalities such as EEG and ECG. The model utilizes a frequency-based tokenization approach, where biosignals are first transformed into spectrogram representations via STFT. Channel-specific positional embedding and temporal positional embedding are added to the tokens to enhance both temporal and spatial representations. These spectral embeddings are then processed using a Linear Attention Transformer.

C.6. ECG Model Experiments

We compare the performance of ECG-JEPA, a time series specific model, and UniTS, a generalized time series model for ECG classifciations. Our ECG experiment and pretrained encoder weights were adopted from the following repositories: `https://github.com/sehunfromdaegu/ecg_jepa` and `https://github.com/mims-harvard/UniTS`.

C.6.1. ECG DATASETS AND PREPROCESSING

We evaluated the models on PTB-XL (Wagner et al., 2020), CPSC (Liu et al., 2018), Chapman-Shaoxing (Zheng et al., 2020), and Ga (Alday et al., 2020). All ECG signals were resampled to 500 Hz and standardized to a length of 2500 timesteps. Samples where the first 15 timesteps contained only zeros across all channels were removed. For ECG-JEPA, the number of ECG channels was reduced from 12 to 8, as the remaining 4 channels can be derived using linear combinations of the selected leads.

For details on dataset access and data splitting, please refer to App. A.

C.6.2. HYPERPARAMETERS AND EXPERIMENTAL PROCEDURES

For the ECG-JEPA model, we use the Adam optimizer (Diederik, 2014) with a learning rate of 1×10^{-3} and a weight decay of 1×10^{-2}. For the UniTS model, we use the Adam optimizer with a learning rate of 1×10^{-4} and a weight decay of 5×10^{-6}. For all experiments, the batch size was set to 32. All experiments were conducted using the PyTorch framework. We report the AUCROC, Sensitivity, and Specificity Score of our experiments in App. D.

C.6.3. ECG MODEL DETAILS

ECG-JEPA (Kim, 2024) is a self-supervised ECG representation learning model that predicts in the latent space rather than reconstructing raw signals. It introduces Cross-Pattern Attention (CroPA), a masked attention mechanism that prioritizes critical ECG features across multiple leads, enhancing performance on downstream tasks.

UniTS (Gao et al., 2024) is a unified multitask time series model that integrates predictive and generative tasks using task tokenization within a single framework. It employs a modified transformer block to learn transferable time series representations across diverse domains, handling variations in sampling rates and temporal patterns.

C.7. Out-of-distribution Experiment Details

In this section, we describe the details on how we ran the OOD transfer experiment, which addresses RQ2. We first define the list of datasets we selected for the transfer experiments, and then explain the detailed procedure of the experiment.

C.7.1. DEFINITION OF OUT-OF-DISTRIBUTION DATASETS

The list of datasets we selected for out-of-distribution (OOD) transfer experiments is described in Table 9. In general, we select the datasets such that they reflect a different task within a modality it was trained on. The OOD may be a novel task

(like COVID-19), a new task (cancer vs pulmonary embolism), or a different granularity of the same task (6-way BI-RADS classification instead of 5-way).

C.7.2. EXPERIMENTAL PROCEDURES

Vision Encoders. For vision encoders, we run a mixed training on the full dataset, with the OOD dataset filtered out.

D. Full Experimental Results

D.1. Full Dataset Multitask Training Results

In this section, we report the detailed model's performance for each dataset in Table 2.

Table 7. **Dataset Classes for Multilabel Classification with CLIMB.**

Dataset	# Classes	Classes
PTB-XL	7	Normal, Conduction Delay (CD), Hypertrophy (HYP), Myocardial Infarction (MI), Sinus Tachycardia/Bradycardia/Conduction (STTC), Atrial Fibrillation/Atrial Flutter (A. Fib/Aflutter), Other
Chapman-Shaoxing	7	Same as PTB-XL
Georgia	7	Same as PTB-XL
CPSC	7	Same as PTB-XL
IIIC	6	Seizure (SZ), Lateralized Periodic Discharges (LPD), Generalized Periodic Discharges (GPD), Lateralized Rhythmic Delta Activity (LRDA), Generalized Rhythmic Delta Activity (GRDA), Other
TUAB	2	Normal, Abnormal
TUEV	6	Spike and Slow Wave (SPSW), Generalized Periodic Epileptiform Discharge (GPED), Periodic Lateralized Epileptiform Discharge (PLED), Eye Movement (EYEM), Artifact (ARTF), Background (BCKG)
MIMIC-CXR	14	Atelectasis, Cardiomegaly, Consolidation, Edema, Enlarged Cardiomediastinum, Fracture, Lung Lesion, Lung Opacity, Pleural Effusion, Pneumonia, Pneumothorax, Pleural Other, Support Devices, No Finding
CheXpert	14	Same as CheXpert
VinDr-CXR	6	Lung tumor, Pneumonia, Tuberculosis, COPD, Other diseases, No finding
COVID-19	4	Normal, Bacterial Pneumonia, COVID-19, Viral Pneumonia
CoronaHack	3	Normal, Bacterial Pneumonia, Viral Pneumonia
VinDr-Mammo	5	BI-RAD 1-5
CBIS-DDSM	6	BI-RAD 0-5
CMMD	2	Benign, Malignant
ISIC-2020	2	Malignant, Benign
HAM10000	5	Melanoma (MEL), Nevus (NV), Basal Cell Carcinoma (BCC), Actinic Keratosis/Intraepithelial Carcinoma (AKIEC), Other (OTHER)
PAD-UFES-20	5	Melanoma (MEL), Nevus (NV), Basal Cell Carcinoma (BCC), Actinic Keratosis/Intraepithelial Carcinoma (AKIEC), Other (OTHER)
Messidor-2	5	None, Mild DR, Moderate DR, Severe DR, PDR
APTOS 2019	5	No DR, Mild, Moderate, Severe, Proliferative DR
Jichi	3	SDR (simple diabetic retinopathy), PPDR (pre-proliferative diabetic retinopathy), PDR (proliferative diabetic retinopathy)
LNDb	3	nodule $\geq$ 3mm, nodule ¡3mm, non-nodule
INSPECT	5	No PE, Acute Subsegmental-only PE, Acute PE, Subsegmental-only PE, Chronic PE
KiTS23	2	Benign, Malignant
Hemorrhage	2	No Hemorrhage, Has Hemorrhage
RSPECT	3	No PE, Chronic PE, Acute PE
EchoNet-Dynamic	-	Not classification
BUSI	3	Normal, Malignant, Benign
COVID-BLUES	2	Has COVID, No COVID
COVID-US	3	Covid, Pneumonia, Normal
Brain Tumor	4	No Tumor, Pituitary Tumor, Glioma Tumor, Meningioma Tumor
Brain MRI	2	Yes, No (presence of tumors)
ABCD	2	Normal, Abnormal
ABIDE	2	ASD, Typical controls
PPMI	2	Control, PD patients
PROTEINS	2	Enzyme, Not enzyme
PPI		
LC25000	5	Colon adenocarcinomas, Benign colon, Lung adenocarcinomas, Lung squamous cell carcinomas, Benign lung
BCSS	4	Tumor, Stroma, Lymphocytic infiltrate, Necrosis/debris
Cholec80		Surgery phase annotations and surgery tool labels
HuGaDB	4	Sitting, Standing, Sitting down, Standing up
Expression Atlas	-	Not classification
Geo	-	Not classification
Vital	-	Not classification
MIMIC-IV	2	48 Hour In-Hospital-Mortality (48 IHM) (Yes/No)

Table 8. **Dataset Demographics and Location Information.**

Dataset	Locations	Demographic Information
PTB-XL	Multiple	sex: 52% male, 48% female; age range: 0-95 (median: 62, IQR: 22); height; weight
Chapman-Shaoxing	Shaoxing, Zhejiang, China	sex: male: 22,599 (56%); female: 17,659 (44%); age groups: 51–60 (19.8%), 61–70 (24%), and 71–80 (17.3%)
Georgia	Emory University, Atlanta, Georgia, USA	age; sex
CPSC	China	unknown
MIMIC-CXR	Beth Israel Deaconess Medical Center in Boston, MA	unknown
CheXpert	Stanford, California, US	sex; age
VinDr-CXR	The Hospital 108 and the Hanoi Medical University Hospital in Vietnam	Training set: median age: 43.77; sex: 52.21% male, 47.79% female; Test set: median age: 31.80; sex: 55.90% male, 44.10% female
VinDr-Mammo	The Institutional Review Board of Hanoi Medical University Hospital (HMUH) and Hospital 108 (H108)	age; imaging device's model
CBIS-DDSM	Stanford, California, US	Unknown
ISIC-2020	Hospital Clínic de Barcelona, Medical University of Vienna, Memorial Sloan Kettering Cancer Center, Melanoma Institute Australia, University of Queensland, and the University of Athens Medical School	sex: female: 15981 (48%), male: 17080 (52%); age range: 0-90 (median: 48.87)
HAM10000	unknown	unknown
PAD-UFES-20	Federal University of Espírito Santo (UFES), Espírito Santo, Brazil	country of parents; age; gender; access to piped water; access to sewage system; region
Messidor-2	Brest University Hospital	unknown
APTOS 2019	Aravind Eye Hospital, India	unknown
Jinchi	Jichi Medical University	unknown
LNDb	Centro Hospitalar e Universitário de São João (CHUSJ) in Porto, Portugal	unknown
ABIDE	California Institute of Technology, Carnegie Mellon University, Kennedy Krieger Institute, and more	age; sex; handedness; full-scale IQ
ABCD	unknown	gender identity; environmental factors
PPMI	Multiple	sex: 54.5% male, 45.5% female; race; age
HuGaDB	unknown	sex: 4 females, 14 males; age: average: 23.67; height: average: 179.06 cm; weight: average: 73.44 kg
INSPECT	Stanford Medicine (2000-2021)	gender: female: 10,733, male: 8,666, unknown: 3; age: 18-39: 2,912, 39-69: 9,974, 69-89: 5,859, ¿89: 657; race: white: 10,704, asian: 2,976, black: 1,103, native: 415, unknown: 2,404; ethnicity: hispanic: 3,018, not hispanic: 15,628, unknown: 756
EchoNet-Dynamic	Stanford University	unknown
BUSI	unknown	unknown
COVID-19	University of Montreal, Canada	unknown
Brain Tumor	Eindhoven University of Technology, Netherlands	unknown
KiTS23	Minnesota, US	unknown
Hemorrhage	Al Hilla Teaching Hospital, Iraq	age: mean: 27.8; gender: male: 46, female: 36
CMMD	China	age
CoronaHack	Mila, University of Montreal	unknown
COVID-BLUES	Maastricht University Medical Center (UMC+) in the Netherlands	weight; sex; height; bmi; age
COVID-US	unknown	gender; age; alcoholic; drug use
IIIC	Massachusetts General Hospital, Harvard Medical School, Boston, USA	1950 patients; labeled by 124 raters; 20 of the raters are physician experts
TUAB	The Temple University Hospital, Philadelphia, Pennsylvania, USA	Evaluation Dataset: Total: 276 files, 253 subjects; Abnormal Female: 63 files, 51 subjects; Abnormal Male: 63 files, 54 subjects; Normal Female: 85 files, 84 subjects; Normal Male: 65 files, 64 subjects; Train Dataset: Total: 2,717 files, 2,130 subjects
TUEV	The Temple University Hospital, Philadelphia, Pennsylvania, USA	290 patients in train; 78 patients in eval
MIMIC-IV	Beth Israel Deaconess Medical Center, Massachusetts Institute of Technology	age; gender; insurance type (medicaid, medicare, other)

Table 9. **Out-of-Distribution Datasets**

Dataset	Classes	Out-of-Distribution Characteristics
COVID-19	Normal, Bacterial Pneumonia, COVID-19, Viral Pneumonia	Novel disease class (COVID-19)
CoronaHack	Normal, Bacterial Pneumonia, Viral Pneumonia, COVID-19	Novel disease class (COVID-19)
CBIS-DDSM	BI-RAD 0-5	More fine-grained classification (6 BI-RADS categories) compared to VinDr-Mammo (5 categories) and CMMD (binary classification)
ISIC-2020	Malignant, Benign	Different task granularity (binary classification)
Jichi	SDR, PPDR, PDR	Different classification scheme for diabetic retinopathy progression compared to Messidor-2 and APTOS 2019's five-stage classification
BCSS	Tumor, Stroma, Lymphocytic infiltrate, Necrosis/debris	Different task type (tissue component classification) compared to LC25000's focus on cancer type classification
BUSI	Normal, Malignant, Benign	Different task focus (breast lesion classification) compared to other ultrasound datasets (COVID-BLUES, COVID-US) which focus on lung pathology
LNDb	nodule $\geq$ 3mm, nodule $<$ 3mm, non-nodule	Different task focus (nodule size classification) compared to other CT datasets like INSPECT and RSPECT which focus on pulmonary embolism
PTB-XL-Finegrained	Normal ECG (NORM), Ischemic in inferior leads (ISCI), Non-specific ST changes (NST_), Ischemic in anterior leads (ISCA), Non-specific ischemic (ISC_), ST-T changes (STTC), Right ventricular hypertrophy (RVH), Right atrial overload/enlargement (RAO/RAE), Septal hypertrophy (SEHYP), Left atrial overload/enlargement (LAO/LAE), Anterior myocardial infarction (AMI), Inferior myocardial infarction (IMI), Lateral myocardial infarction (LMI), Posterior myocardial infarction (PMI), Left anterior/left posterior fascicular block (LAFB/LPFB), Incomplete right bundle branch block (IRBBB), AV block (_AVB), Non-specific intraventricular conduction disturbance (IVCD), Complete right bundle branch block (CRBBB), Complete left bundle branch block (CLBBB), Wolff-Parkinson-White syndrome (WPW), Incomplete left bundle branch block (ILBBB)	More fine-grained classification (24 categories) compared to PTB-XL superclass (7 categories in BenchMD).
TUEV	Spike and slow wave (SPSW), Generalized periodic epileptiform discharge (GPED), Periodic lateralized epileptiform discharge (PLED), Eye movement (EYEM), artifact (ARTF), and Background (BCKG)	Data consists of pathological patterns, human artifacts, and normal background activity.

Table 10. **Performance metrics of MedVit across different medical imaging datasets.**
MedVit

Dataset	AUC	Sensitivity	Specificity	F1 Score	Accuracy
CT RSPECT	0.7609	0.3333	0.6667	0.3248	0.9667
CT INSPECT	0.5495	0.2000	0.8000	0.1764	0.9156
MIMIC-CXR	0.6743	0.1447	0.9432	0.1444	0.8737
Fundus JICHI	0.5464	0.2500	0.7625	0.1951	0.8077
Fundus APTOS	0.4141	0.2000	0.8000	0.0750	0.6923
CT LNDB	0.7009	0.4960	0.4960	0.4395	0.7841
ISIC 2020	0.2676	0.5000	0.5000	0.4931	0.9726
CBIS-DDSM	0.8333	0.5000	0.5000	0.3000	0.4286
BUSI	0.1111	0.5000	0.5000	0.3333	0.5000
LC25000	0.9448	0.4444	0.8631	0.3218	0.7836
HAM10000	0.6446	0.2500	0.7500	0.2143	0.8750
VinDr CXR	0.6546	0.1607	0.9005	0.1278	0.8587
CoronaHack	0.6907	0.4583	0.7526	0.4242	0.7333
BCSS	0.5833	0.3333	0.6667	0.2727	0.7949
VinDr Mammo	0.4205	0.3333	0.6667	0.2716	0.7917
COVID-BLUES	0.3556	0.5000	0.5000	0.3448	0.5263
Brain Tumor	0.8927	0.4375	0.8229	0.3167	0.7500
KiTS23	0.4063	0.5000	0.5000	0.4706	0.8889
CheXpert	0.6333	0.1686	0.9021	0.1693	0.8455
PAD-UFES-20	0.6528	0.3333	0.6667	0.0667	0.4074
COVID-19 CXR	0.6972	0.3333	0.6667	0.2222	0.6667
COVID-US	0.8889	0.5000	0.7500	0.3556	0.6000
Messidor-2	0.0000	0.5000	0.5000	0.4286	0.7500
Overall	0.5793	0.3642	0.6903	0.2821	0.7484

Table 11. **Performance metrics of PMC CLIP across different medical imaging datasets.**
PMC CLIP

Dataset	AUC	Sensitivity	Specificity	F1 Score	Accuracy
CT RSPECT	0.7928	0.3333	0.6667	0.3241	0.9639
CT INSPECT	0.5484	0.2000	0.8000	0.1779	0.9205
MIMIC-CXR	0.6613	0.1261	0.9411	0.1234	0.8438
Fundus JINCHI	0.5492	0.2560	0.7513	0.2110	0.8308
Fundus APTOS	0.5863	0.2033	0.8023	0.0928	0.7124
CT LNDB	0.7012	0.5000	0.5000	0.4515	0.8232
ISIC 2020	0.7351	0.5000	0.5000	0.4955	0.9823
CBIS-DDSM	0.6475	0.2069	0.8064	0.1798	0.8024
BUSI	0.5371	0.3233	0.6596	0.2847	0.6616
LC25000	0.9842	0.7328	0.9332	0.7058	0.8931
HAM10000	0.7439	0.2191	0.8050	0.1921	0.8670
VinDr CXR	0.6233	0.0935	0.9235	0.0720	0.9110
CoronaHack	0.8480	0.5062	0.7729	0.4458	0.7212
BCSS	0.6432	0.2555	0.7534	0.1855	0.7289
VinDr Mammo	0.5807	0.2062	0.8007	0.1685	0.8651
COVID-BLUES	0.4175	0.4941	0.4941	0.2304	0.2708
Brain Tumor	0.6160	0.3210	0.7771	0.2656	0.6802
KiTS23	0.4712	0.5000	0.5000	0.4658	0.8718
CheXpert	0.6680	0.1170	0.9191	0.1287	0.7665
PAD-UFES-20	0.5427	0.2552	0.8121	0.1436	0.7089
COVID-19 CXR	0.8240	0.4106	0.8579	0.3550	0.8138
CMMD	0.6140	0.5226	0.5226	0.0499	0.0513
COVID-US	0.6091	0.3333	0.6730	0.1961	0.6000
Messidor-2	0.3898	0.2000	0.8000	0.1473	0.8331
CT Hemorrhage	0.5805	0.5000	0.5000	0.4550	0.8350
Brain Tumor 2	0.5848	0.5441	0.5441	0.5433	0.5882
Overall	0.6346	0.3408	0.7237	0.2727	0.7518

Table 12. **Performance metrics of RAD-DINO across different medical imaging datasets.**
RAD-DINO

Dataset	AUC	Sensitivity	Specificity	F1 Score	Accuracy
CT RSPECT	0.8357	0.3333	0.6667	0.3241	0.9639
CT INSPECT	0.5752	0.2000	0.8000	0.1779	0.9205
MIMIC-CXR	0.7281	0.1873	0.9404	0.2034	0.8583
Fundus JICHI	0.6093	0.2500	0.7500	0.1988	0.8301
Fundus APTOS	0.6589	0.2000	0.8000	0.1320	0.7970
CT LNDB	0.6950	0.5000	0.5000	0.4515	0.8232
ISIC 2020	0.7753	0.4999	0.4999	0.4955	0.9822
CBIS-DDSM	0.5935	0.1988	0.8015	0.1438	0.8225
BUSI	0.6570	0.3333	0.6667	0.2389	0.7056
LC25000	0.9809	0.6853	0.9213	0.6288	0.8741
HAM10000	0.8128	0.2392	0.8221	0.2337	0.8752
VinDr CXR	0.7605	0.1179	0.9376	0.1003	0.9152
CoronaHack	0.9173	0.6078	0.7995	0.5739	0.7436
BCSS	0.6502	0.2622	0.7535	0.1526	0.6768
VinDr Mammo	0.5756	0.2000	0.8000	0.1606	0.8682
COVID-BLUES	0.5775	0.5000	0.5000	0.2066	0.2604
Brain Tumor	0.6725	0.3334	0.7760	0.2437	0.6459
KiTS23	0.4565	0.5000	0.5000	0.4658	0.8718
CheXpert	0.7516	0.2124	0.9264	0.2347	0.8068
PAD-UFES-20	0.6125	0.2666	0.8217	0.1722	0.7028
COVID-19 CXR	0.8946	0.4199	0.8357	0.3952	0.7753
CMMD	0.5065	0.5000	0.5000	0.0064	0.0064
COVID-US	0.6750	0.5803	0.7397	0.5056	0.6800
Messidor-2	0.5311	0.2000	0.8000	0.1473	0.8331
CT Hemorrhage	0.7054	0.5000	0.5000	0.4550	0.8350
Brain Tumor 2	0.5519	0.5000	0.5000	0.2500	0.3333
Overall	0.6831	0.3588	0.7253	0.2807	0.7464

Table 13. **Performance metrics of SBB2 across different medical imaging datasets.**
SBB2

Dataset	AUC	Sensitivity	Specificity	F1 Score	Accuracy
CT RSPECT	0.8556	0.3343	0.6676	0.3260	0.9640
CT INSPECT	0.5624	0.2000	0.8000	0.1779	0.9204
MIMIC-CXR	0.7227	0.1714	0.9429	0.1875	0.8561
Fundus JINCHI	0.7215	0.3261	0.7697	0.3071	0.8389
Fundus APTOS	0.8212	0.3514	0.8927	0.3292	0.8647
CT LNDB	0.6932	0.5000	0.5000	0.4515	0.8232
ISIC 2020	0.8026	0.5000	0.5000	0.4955	0.9823
CBIS-DDSM	0.6366	0.1994	0.8007	0.1437	0.8232
BUSI	0.6649	0.3561	0.6773	0.3040	0.7056
LC25000	0.9977	0.9622	0.9906	0.9622	0.9849
HAM10000	0.8641	0.2797	0.8438	0.2902	0.8824
VinDr CXR	0.6377	0.0845	0.9188	0.0717	0.9261
CoronaHack	0.9127	0.7521	0.8830	0.7532	0.8462
BCSS	0.7249	0.4504	0.8171	0.3938	0.7550
VinDr Mammo	0.5981	0.2003	0.8013	0.1668	0.8653
COVID-BLUES	0.6890	0.5977	0.5977	0.6063	0.7500
Brain Tumor	0.7723	0.5411	0.8434	0.4945	0.7640
KiTS23	0.6137	0.5000	0.5000	0.4658	0.8718
CheXpert	0.7325	0.2204	0.9238	0.2520	0.8027
PAD-UFES-20	0.6844	0.3048	0.8280	0.2064	0.7264
COVID-19 CXR	0.9487	0.7784	0.9393	0.7951	0.9216
CMMD	0.3803	0.3871	0.3871	0.4348	0.7692
COVID-US	0.7789	0.5318	0.7921	0.5258	0.7333
Messidor-2	0.6529	0.2000	0.8000	0.1473	0.8331
CT Hemorrhage	0.7307	0.4815	0.4815	0.4583	0.7883
Brain Tumor 2	0.7734	0.7059	0.7059	0.7230	0.7843
Overall	0.7297	0.4199	0.7540	0.4027	0.8378

Table 14. **Performance metrics of Swin Transformer across different medical imaging datasets.**
Swin Transformer

Dataset	AUC	Sensitivity	Specificity	F1 Score	Accuracy
CT RSPECT	0.8962	0.4318	0.7605	0.4613	0.9683
CT INSPECT	0.6468	0.2049	0.8035	0.1878	0.9219
MIMIC-CXR	0.7620	0.1748	0.9459	0.2113	0.8571
Fundus JICHI	0.7821	0.3663	0.7967	0.3392	0.8396
Fundus APTOS	0.8636	0.3632	0.9089	0.3123	0.8849
CT LNDB	0.6660	0.5113	0.5113	0.4778	0.8239
ISIC 2020	0.7654	0.5313	0.5313	0.5438	0.9780
CBIS-DDSM	0.7078	0.2019	0.7973	0.1688	0.8071
BUSI	0.6264	0.3627	0.6742	0.1955	0.5228
LC25000	0.9987	0.9573	0.9893	0.9572	0.9829
HAM10000	0.8764	0.3743	0.8557	0.3842	0.8860
VinDr CXR	0.6206	0.0920	0.9210	0.0811	0.9248
CoronaHack	0.9231	0.7725	0.8909	0.7580	0.8419
BCSS	0.7141	0.3573	0.7713	0.2427	0.6434
VinDr Mammo	0.6330	0.2000	0.8000	0.1606	0.8682
COVID-BLUES	0.6175	0.5989	0.5989	0.6069	0.7708
Brain Tumor	0.8555	0.6215	0.8729	0.6311	0.8160
KiTS23	0.4621	0.5000	0.5000	0.4658	0.8718
CheXpert	0.7395	0.2009	0.9438	0.2395	0.8140
PAD-UFES-20	0.8042	0.3996	0.8542	0.3654	0.8100
COVID-19 CXR	0.9319	0.7029	0.9268	0.7396	0.8978
CT Hemorrhage	0.7562	0.5000	0.5000	0.4550	0.8350
COVID-US	0.8721	0.6727	0.8619	0.6672	0.8133
Messidor-2	0.6645	0.2524	0.8072	0.2183	0.8366
Brain Tumor 2	0.9360	0.5588	0.5588	0.5149	0.7059
Overall	0.7649	0.4364	0.7753	0.4154	0.8369

Table 15. **Performance metrics of EVA-2 across different medical imaging datasets.**
EVA-2

Dataset	AUC	Sensitivity	Specificity	F1 Score	Accuracy
Fundus JINCHI	0.6808	0.2500	0.7500	0.5250	0.8301
COVID-19 CXR	0.9007	0.4372	0.8751	0.6081	0.8335
ISIC 2020	0.7291	0.5000	0.5000	0.9736	0.9823
HAM10000	0.8003	0.2625	0.8204	0.5575	0.8684
MIMIC-CXR	0.7636	0.2018	0.9291	0.3616	0.8546
Brain Tumor	0.6221	0.3531	0.7756	0.2297	0.6523
CT LNDB	0.6405	0.5000	0.5000	0.7434	0.8232
CBIS-DDSM	0.5590	0.2916	0.8046	0.4000	0.8151
VinDr Mammo	0.5240	0.2013	0.8002	0.5388	0.8683
CT Hemorrhage	0.6970	0.5000	0.5000	0.7599	0.8350
KiTS23	0.6337	0.5196	0.5196	0.0958	0.1624
VinDr CXR	0.6986	0.1136	0.9326	0.4718	0.9223
Messidor-2	0.5972	0.2000	0.8000	0.4293	0.8331
CoronaHack	0.8826	0.4654	0.7472	0.4578	0.6902
Fundus APTOS	0.8674	0.2773	0.8562	0.4195	0.8117
PAD-UFES-20	0.5795	0.2386	0.8073	0.2656	0.7673
CheXpert	0.8056	0.2596	0.8940	0.3897	0.8034
CMMD	0.4932	0.5000	0.5000	0.0001	0.0064
BUSI	0.5925	0.3333	0.6667	0.4001	0.7056
Brain Tumor 2	0.6739	0.5000	0.5000	0.5333	0.6667
Overall	0.6871	0.3452	0.7239	0.4580	0.7366

Table 16. **Performance metrics of ConvNextv2 across different medical imaging datasets.**

ConvNextv2

Dataset	AUC	Sensitivity	Specificity	F1 Score	Accuracy
CT RSPECT	0.9400	0.5598	0.8337	0.6080	0.9748
CT INSPECT	0.5867	0.2098	0.8084	0.1983	0.9217
MIMIC-CXR	0.7997	0.2400	0.9480	0.2740	0.8721
Fundus JICHI	0.8568	0.5949	0.8492	0.5997	0.8798
Fundus APTOS	0.9380	0.5835	0.9455	0.6105	0.9214
CT LNDB	0.6670	0.5311	0.5311	0.5322	0.7722
ISIC 2020	0.8529	0.5042	0.5042	0.5039	0.9823
CBIS-DDSM	0.7070	0.2435	0.8170	0.2214	0.8299
BUSI	0.7653	0.4862	0.7431	0.4623	0.6853
LC25000	0.9999	0.9926	0.9982	0.9926	0.9971
HAM10000	0.9423	0.6485	0.9298	0.6511	0.9251
VinDr CXR	0.5609	0.0852	0.9175	0.0726	0.9270
CoronaHack	0.9573	0.8369	0.9260	0.8381	0.9017
BCSS	0.8098	0.5076	0.8180	0.4981	0.7773
VinDr Mammo	0.6732	0.2536	0.8069	0.2414	0.8693
COVID-BLUES	0.7318	0.6814	0.6814	0.6742	0.7396
Brain Tumor	0.9293	0.7257	0.9069	0.7136	0.8655
KiTS23	0.4108	0.5000	0.5000	0.4658	0.8718
CheXpert	0.8037	0.2722	0.9521	0.3160	0.8236
PAD-UFES-20	0.9068	0.5511	0.8978	0.5873	0.8693
COVID-19 CXR	0.9639	0.7474	0.9495	0.7545	0.9337
CMMD	-	0.4935	0.4935	0.4951	0.9808
COVID-US	0.8254	0.7561	0.8841	0.7313	0.8400
Messidor-2	0.8245	0.5116	0.8684	0.5116	0.8606
CT Hemorrhage	0.7485	0.5306	0.5306	0.5188	0.8388
Brain Tumor 2	0.9585	0.9265	0.9265	0.9328	0.9412
Overall	0.7867	0.5374	0.8064	0.5387	0.8770

Table 17. **Performance metrics of InternViT across different medical imaging datasets.**

InternViT

Dataset	AUC	Sensitivity	Specificity	F1 Score	Accuracy
CT RSPECT	0.9005	0.4407	0.7597	0.4791	0.9679
CT INSPECT	0.5954	0.2013	0.8008	0.1808	0.9206
MIMIC-CXR	0.7780	0.2196	0.9426	0.2397	0.8667
Fundus JINCHI	0.8258	0.5438	0.8224	0.4625	0.7293
Fundus APTOS	0.8786	0.4505	0.9260	0.4115	0.8941
CT LNDB	0.6810	0.5448	0.5448	0.5470	0.8050
ISIC 2020	0.8427	0.5040	0.5040	0.5037	0.9820
CBIS-DDSM	0.6701	0.2714	0.8217	0.2488	0.8205
BUSI	0.7310	0.5016	0.7391	0.4475	0.6311
LC25000	0.9990	0.9738	0.9934	0.9737	0.9895
HAM10000	0.9012	0.6092	0.9210	0.5381	0.8820
VinDr CXR	0.6309	0.0899	0.9184	0.0808	0.9272
CoronaHack	0.9303	0.7680	0.8910	0.7515	0.8419
BCSS	0.7856	0.4696	0.8235	0.3876	0.7584
VinDr Mammo	0.6450	0.2473	0.8176	0.2423	0.7962
COVID-BLUES	0.6772	0.6592	0.6592	0.6364	0.6875
Brain Tumor	0.8236	0.6134	0.8734	0.5869	0.8135
KiTS23	0.5722	0.5000	0.5000	0.4658	0.8718
CheXpert	0.7830	0.2333	0.9502	0.2757	0.8168
PAD-UFES-20	0.8600	0.5162	0.8844	0.5476	0.8501
COVID-19 CXR	0.9526	0.7525	0.9484	0.7360	0.9281
CMMD	0.2817	0.5000	0.5000	0.4984	0.9936
COVID-US	0.7978	0.4864	0.7556	0.4680	0.7067
Messidor-2	0.8119	0.2977	0.8050	0.1526	0.6720
CT Hemorrhage	0.7790	0.6562	0.6562	0.6398	0.7806
Brain Tumor 2	0.9377	0.7500	0.7500	0.7733	0.8235
Overall	0.7720	0.4923	0.7888	0.4721	0.8368

Table 18. **Performance evaluation of GCN across different modalities and datasets.**

GCN

Modality	Dataset	Performance Metrics		
		AUC	Sensitivity	Specificity
Brain Networks	PPMI	0.973	0.922	0.897
	ABIDE	0.626	0.596	0.586
	ABCD	0.814	0.570	0.916
	Average	0.804	0.696	0.800
Molecular	PPI	0.807	0.496	0.716
	PROTEINS	0.718	0.568	0.803
	Average	0.763	0.532	0.760
Overall	Average	0.783	0.614	0.780

Table 19. **Performance evaluation of GAT across different modalities and datasets.**

GAT

Modality	Dataset	AUC	Sensitivity	Specificity
		Performance Metrics		
Brain Networks	PPMI	0.927	0.931	0.828
	ABIDE	0.688	0.818	0.385
	ABCD	0.500	1.000	0.000
	Average	0.705	0.916	0.404
Molecular	PPI	0.926	0.572	0.798
	PROTEINS	0.719	0.529	0.803
	Average	0.823	0.551	0.801
Overall	Average	0.764	0.733	0.602

Table 20. **Performance evaluation of Graph Transformers across different modalities and datasets.**

Graph Transformers

Modality	Dataset	AUC	Sensitivity	Specificity
		Performance Metrics		
Brain Networks	PPMI	0.950	0.862	0.957
	ABIDE	0.743	0.707	0.683
	ABCD	0.864	0.860	0.837
	Average	0.852	0.810	0.826
Molecular	PPI	0.997	0.606	0.873
	PROTEINS	0.580	0.156	0.967
	Average	0.789	0.381	0.920
Overall	Average	0.820	0.595	0.873

Table 21. **Performance metrics across different medical imaging datasets.**
ConvNextv2 (Single Task Training)

Dataset	AUC	Sensitivity	Specificity	F1 Score	Accuracy
CT RSPECT	0.9680	0.7388	0.9096	0.7472	0.9675
CT INSPECT	0.5524	0.2170	0.8103	0.2070	0.7930
MIMIC-CXR	0.8036	0.8100	0.6526	0.3735	0.6805
Fundus JINCHI	0.8994	0.6689	0.8794	0.6465	0.7763
Fundus APTOS	0.9162	0.4880	0.9309	0.4969	0.7613
CT LNDB	0.6750	0.4983	0.4983	0.4507	0.8204
ISIC 2020	0.8936	0.4957	0.9559	0.6120	0.9478
CBIS-DDSM	0.6375	0.2173	0.8070	0.1837	0.5563
BUSI	0.6370	0.4359	0.7013	0.4064	0.5381
LC25000	1.0000	0.9971	0.9993	0.9971	0.9971
HAM10000	0.9531	0.7154	0.9416	0.6850	0.8018
VinDr CXR	-	0.3353	0.5809	0.1281	0.7099
CoronaHack	0.9461	0.8404	0.9225	0.8400	0.8462
BCSS	0.8431	0.6276	0.8571	0.6053	0.6219
VinDr Mammo	0.6864	0.3138	0.8179	0.2802	0.6747
COVID-BLUES	0.5282	0.5000	0.5000	0.2066	0.2604
Brain Tumor	0.8291	0.4801	0.8188	0.4555	0.4721
KiTS23	0.3235	0.5000	0.5000	0.4658	0.8718
CheXpert	-	0.6351	0.7669	0.4516	0.7603
PAD-UFES-20	0.8112	0.3295	0.8531	0.3430	0.5425
COVID-19 CXR	0.9168	0.5689	0.8947	0.6013	0.7419
CMMD	0.5204	0.4860	0.4860	0.4913	0.9658
COVID-US	0.5000	0.3333	0.6667	0.0920	0.1600
Messidor-2	0.8301	0.2590	0.8073	0.2117	0.5886
CT Hemorrhage	0.7666	0.8884	0.2471	0.5724	0.7825
Brain Tumor 2	0.7734	0.0000	1.0000	0.4000	0.6667

Table 22. **Performance metrics of Llava-Med across different medical imaging datasets.** Note the overall row is averaged across dataset, which is different from the modality-wise average in Table 4.

Llava-Med

Dataset	Zero-Shot				Fine-Tuned			
	Accuracy	Sensitivity	Specificity	F1 Score	Accuracy	Sensitivity	Specificity	F1 Score
MIMIC-CXR	0.001	0.214	0.786	0.063	0.001	0.214	0.794	0.090
CheXpert	0.000	0.077	0.924	0.036	0.000	0.154	0.847	0.093
VinDr-CXR	0.045	0.083	0.916	0.016	0.702	0.083	0.917	0.069
COVID-19	0.009	0.250	0.750	0.005	0.455	0.250	0.750	0.156
CoronaHack	0.388	0.333	0.667	0.186	0.388	0.333	0.667	0.186
Brain Tumor	0.393	0.445	0.799	0.300	0.292	0.250	0.750	0.113
Brain Tumor 2	0.333	0.500	0.500	0.250	0.667	0.500	0.500	0.400
BUSI	0.579	0.391	0.697	0.357	0.558	0.333	0.667	0.239
COVID-BLUES	0.365	0.557	0.557	0.353	0.740	0.500	0.500	0.425
COVID-US	0.400	0.333	0.667	0.190	0.440	0.333	0.667	0.204
CBIS	0.008	0.202	0.799	0.005	0.560	0.200	0.800	0.144
VinDr-Mammo	0.047	0.200	0.800	0.018	0.670	0.200	0.800	0.161
CMMD	0.091	0.206	0.800	0.045	0.994	0.500	0.500	0.498
ISIC 2020	0.982	0.500	0.500	0.496	0.982	0.333	0.667	0.330
HAM10000	0.110	0.201	0.800	0.047	0.670	0.201	0.800	0.162
PAD-UFES-20	0.307	0.186	0.800	0.107	0.368	0.200	0.800	0.108
Messidor-2	0.151	0.157	0.832	0.048	0.583	0.200	0.800	0.147
APTOS	0.492	0.200	0.800	0.132	0.492	0.200	0.800	0.132
Jichi	0.660	0.250	0.750	0.199	0.660	0.250	0.750	0.199
LNDb	0.823	0.500	0.500	0.452	0.645	0.541	0.541	0.520
Kits23	0.128	0.500	0.500	0.114	0.872	0.500	0.500	0.466
Brain CT	0.835	0.500	0.500	0.455	0.835	0.500	0.500	0.455
INSPECT	0.004	0.194	0.800	0.006	0.801	0.200	0.800	0.178
Cholec 80	0.000	1.000	0.000	0.243	0.296	0.143	0.857	0.069
Overall	0.298	0.333	0.685	0.172	0.570	0.297	0.707	0.231

Table 23. **Model Performance on Different EEG Datasets**

Model Name	IIIC				TUEV				TUAB				Overall			
	AUC	Sens	Spe	F1	AUC	Sens	Spe	F1	AUC	Sens	Spe	F1	AUC	Sens	Spe	F1
SPARCNet	.846	.525	.905	.589	.801	.495	.877	.286	.868	.796	.796	.797	.838	.605	.859	.557
CNNTransformer	.809	.435	.890	.399	.874	.473	.913	.386	.879	.797	.797	.799	.854	.569	.867	.528
FFCL	.841	.458	.805	.448	.801	.443	.906	.347	.874	.787	.787	.789	.839	.562	.833	.528
ContraWR	.832	.446	.892	.410	.847	.439	.898	.370	.872	.782	.782	.781	.850	.556	.858	.520
STTransformer	.785	.412	.884	.407	.701	.371	.874	.262	.864	.785	.785	.787	.783	.522	.848	.485
BIOT	.854	.510	.905	.499	.856	.466	.908	.371	.879	.798	.798	.799	.863	.591	.870	.556
BIOT-pretrain-PREST	.844	.496	.902	.486	.898	.580	.918	.373	.878	.797	.797	.799	.873	.624	.872	.552
BIOT-pretrain-SHHS+PREST	.848	.523	.906	.507	.880	.586	.914	.415	.882	.806	.806	.808	.870	.639	.875	.577
BIOT-pretrain-six-datasets	.862	.546	.911	.531	.878	.549	.917	.397	.869	.794	.794	.795	.870	.630	.874	.574

Table 24. **Model Performance of BIOT Variants with TUEV Finetuning**

Pretrain Encoder	Num Shots	Finetune	AUC	Sens	Spec
BIOT	1	TUEV	.589	.232	.841
	8		.688	.298	.859
	32		.740	.359	.873
	full		.856	.466	.908
BIOT-pretrain-PREST	1	TUEV	.609	.239	.835
	8		.754	.372	.871
	32		.781	.363	.899
	full		.898	.580	.918
BIOT-pretrain-SHHS+PREST	1	TUEV	.630	.239	.836
	8		.723	.305	.861
	32		.777	.382	.879
	full		.880	.586	.914
BIOT-pretrain-IIIC+TUEV	1	TUEV	.553	.179	.836
	8		.759	.332	.873
	32		.807	.410	.894
	full		.869	.510	.905

Table 25. **Model Performance on Different ECG Datasets**

Model Name	PTB-XL			ChapmanShao			CPSC			Ga			Overall		
	AUC	Sens	Spe	AUC	Sens	Spe	AUC	Sens	Spe	AUC	Sens	Spe	AUC	Sens	Spe
Transformer	.785	.239	.885	.797	.312	.919	.579	.213	.883	.671	.251	.891	.708	.253	.895
ECG-JEPA	.906	.591	.918	.858	.392	.935	.979	.797	.980	.767	.294	.899	.877	.518	.877
UniTS	.669	.150	.861	.656	.146	.859	.641	.143	.857	.598	.158	.863	.641	.149	.860

Table 26. **Model Performance of ECG-JEPA and UniTS Variants with PTB-XL Finetuning**. Ours is the model pretrained on CLIMB dataset with PTB-XL removed.

Model	Pretrain Encoder	Num Shots	Finetune	AUC	Sens	Spe
ECG-JEPA	Ours	1	PTB-XL	.633	.048	.956
		8		.760	.113	.966
		full		.895	.210	.980
	PTB-XL	1	PTB-XL	.512	.043	.956
		8		.472	.043	.956
		full		.868	.195	.979
UniTS	Ours	1	PTB-XL	.527	.430	.537
		8		.549	.641	.370
		full		.673	.025	.993
	PTB-XL	1	PTB-XL	.512	.674	.371
		8		.470	.322	.658
		full		.688	.053	.984

Table 27. **Model Performance of ECG-JEPA Variants with Different Pretraining.** Ours is the model pretrained on CLIMB dataset.

Pretrain	Finetuned	AUC	Sens	Spe
PTB-XL	PTB-XL	.776	.237	.883
CPSC	CPSC	.682	.144	.857
ChapmanShao	ChapmanShao	.771	.248	.899
Ga	Ga	.474	.143	.857
	PTB-XL	.805	.329	.902
	CPSC	.843	.343	.918
Ours	ChapmanShao	.831	.355	.932
	Ga	.704	.273	.894

Table 28. **Model Performance of UniTS Variants with Different Pretraining.** Ours is the model pretrained on CLIMB dataset and Original is the pretrained encoder provided by the UniTS model.

Pretrain	Train	Eval	AUC	Sens	Spe
	PTB-XL	PTB-XL	.669	.150	.861
Original	CPSC	CPSC	.641	.143	.857
	ChapmanShao	ChapmanShao	.656	.146	.859
	Ga	Ga	.598	.158	.863
		PTB-XL	.772	.242	.886
Original	Ours	CPSC	.871	.336	.919
		ChapmanShao	.812	.333	.927
		Ga	.742	.271	.894

Table 29. **Performance Comparison with Dataset Specific Encoders.** Ours is the result of multitask universal encoders trained on CLIMB, whereas Dataset SoTA is the state-of-the-art encoder specially tuned and optimized for that particular task. Note we aim to preserve as much information as possible from each datasets and avoids binning classes, so the task for some datasets, like VinDr-CXR and CBIS-DDSM, may be different from the ones used in other works. The results are taken directly from the papers.

Dataset	Ours (AUC)	Dataset SoTA (AUC)	Source/Method Name	Reference
PTB-XL	0.895	0.896	ECG JEPA	Link
Chapman-Shaoxing	0.858	0.979	X3ECG w/ HC + DDI	–
Georgia	0.767	–	–	–
CPSC	0.978	0.974	ECG JEPA	Link
MIMIC-CXR	0.800	0.834	ChexClusion	Link
CheXpert	0.783	0.933	CFT	Link
VinDr-CXR	0.631 (14 classes)	0.961 (6 classes)	Paper	Link
VinDr-Mammo	0.673 (5 classes)	0.840 (2 classes)	MaMT4	Link
CBIS-DDSM	0.707 (5 classes)	0.900 (2 classes)	MEWOA	Link
ISIC 2020	0.853	0.943	Kaggle Leaderboard	Link
HAM10000	0.942	0.943	Paper	Link
PAD-UFES-20	0.907	0.920	EfficientNetB3	Link
Messidor-2	0.825 (5 classes)	0.971 (2 classes)	Paper	Link
APTOS 2019	0.938	0.920	Survey	Link
Jichi	0.857	–	–	–
LNDb	0.681	0.831 (Fleischner_kw)	Leaderboard	Link
INSPECT	0.595	0.771 (Accuracy)	Paper	Link
BUSI	0.765	–	–	–
COVID-19	0.964	–	–	–
Brain Tumor	0.929	–	–	–
Brain MRI	0.959	–	–	–
Kits23	0.572	0.835 (DICE)	Leaderboard	Link
Hemorrhage	0.779	–	–	–
CoronaHack	0.957	–	–	–
COVID-BLUES	0.732	–	–	–
COVID-US	0.825	0.94	Review	Link
IIIC	0.862	0.580 (Balanced Acc.)	–	–
TUAB	0.882	0.882	–	–
TUEV	0.898	0.528 (Balanced Acc.)	–	–
PROTEINS	0.719	0.849 (Acc)	HGP-SL	Link
PPI	0.997	0.997 (Acc)	g2-MLP	Link
RSPECT	0.94	–	–	–
LC25000	1.000	1.000	SE Networks	Link
BCSS	0.810	0.710 (mIoU)	MLP-MF	Link